1968

Describing Function Analysis of the Field-effect Transistor Oscillator

Edward C. H. Chang

DESCRIBING-FUNCTION ANALYSIS OF THE FIELD-EFFECT TRANSISTOR OSCILLATOR

BY

EDWARD C. H. CHANG

A thesis submitted
in partial fulfillment of the requirements for the
degree Master of Science, Department of
Electrical Engineering, South Dakota
State University

1968

DESCRIBING-FUNCTION ANALYSIS OF THE

FIELD-EFFECT TRANSISTOR OSCILLATOR

This thesis is approved as a creditable and independent investigation by a candidate for the degree, Master of Science, and is acceptable as meeting the thesis requirements for this degree, but without implying that the conclusions reached by the candidate are necessarily the conclusions of the major department.

Thesis Adviser Date

Head, Electrical Engineering Department Date

ACKNOWLEDGMENTS

The author wishes to express his appreciation and gratitude to Dr. F. C. Fitchen, whose guidance and advice made this investigation possible, and to the National Science Foundation for partial support of this investigation.

E.C.H.C.

TABLE OF CONTENTS

LIST OF TABLES

LIST OF FIGURES

Figure Page

CHAPTER I

INTRODUCTION

Although the field-effect, or unipolar, transistor was the earliest known active semiconductor device, it was relatively neglected for many years. The bipolar or conventional transistor dominated the field of electronics. But, because of high-input impedance, low self-generated noise, and greater resistance to nuclear radiation the field-effect transistor became the subject of intensive research. Recently, due to advances in fabrication techniques, it has become possible to manufacture field-effect transistors having electrical properties which make them very attractive for circuit applications.

In the bipolar transistor both positive and negative free carriers take part in the functioning of the device; hence the name bipolar. In the bipolar device, the charge of excess minority carriers injected into the base region is compensated by an equal charge of majority carriers so that electrical neutrality in the base region is maintained. On the other hand, in unipolar devices, the current is carried only by the free majority carriers in the conducting channel and no essential role is played by the small number of minority carriers; hence the name unipolar. The number of carriers available to carry current in the conducting region of the unipolar device is controlled by the application of an electric field to the junction interface. In the junction gate field-effect

transistor shown in Figure 1, the gate is a layer of semiconductor of a conductivity type (p-type) opposite to that of the channel (n-type). The junction gate is reverse biased with respect to the channel forming an insulating depletion layer which encroaches upon the conducting channel, effectively limiting its dimensions. A more negative voltage on the gate will further reduce the channel, reducing its conductance; a less negative voltage will let the channel expand, increasing its conductance. At a particular gate-source voltage, the pinch-off voltage, the channel conductance is reduced to a negligible extent.

The field-effect transistor exhibits nonlinear properties, and thus is similar to other electronic active devices. It is the opinion of the great majority of workers in the field of nonlinear systems that a general method of analysis or synthesis for nonlinear problems is impossible. It is possible, however, to develop a series of analyses that apply to restricted classes of nonlinearities according to their usefulness. The describing-function technique has been known as an effective tool for the analysis of relay or on-off devices. A gradual refining of this technique is apparent and wider application is also possible. With the help of the Nyquist criterion, the nonlinear problem of oscillation can also be solved by employing the describing-function method. This technique of analysis is based on the well-known method of "equivalent linearization or harmonic balance" which was advocated by N. Krylov

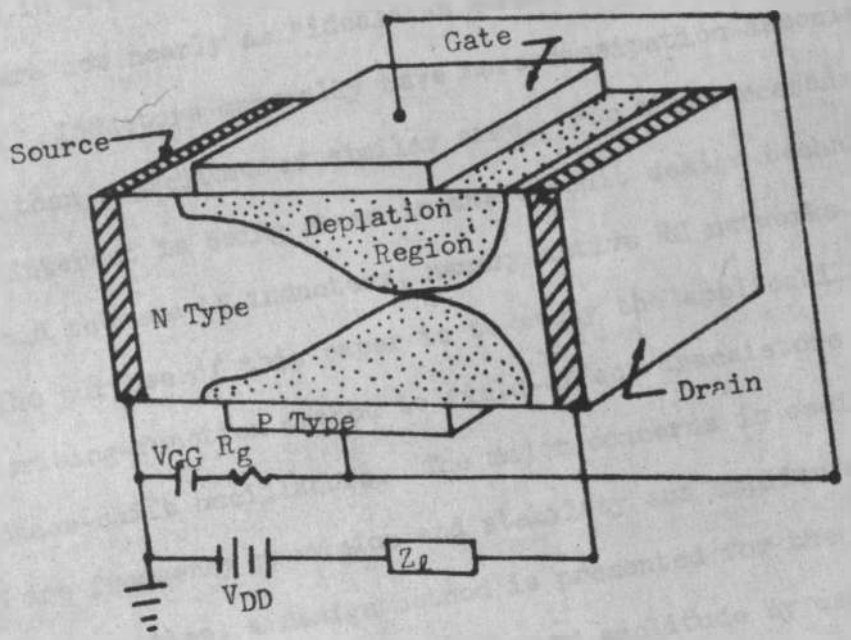

Figure 1. Schematic Diagram of a Unipolar Field-Effect Transistor

and N. Bogoliubov. E. P. Popov, J. E. Gibson, and W. J. Cunningham also exploited its applicability to nonlinear control systems.

The subject of active RC networks is also one that attracts considerable attention from network theorists. There are two major reasons. First, the inductor is a relatively large and heavy element in comparison with the capacitor. This is especially true at frequencies in the audio range. Second, commercially available inductors are not nearly as "ideal" as commercially available capacitors. Inductors generally have more dissipation associated with them than capacitors of similar size. For these reasons more and more interest is being shown in the circuit design techniques which avoid the use of inductors, namely active RC networks.

The purpose of this paper is to study the applicability of the describing-function method to field-effect transistors employed in RC phase-shift oscillators. The major concerns in oscillator design are frequency precision and stability and amplitude of oscillation. Also, a design method is presented for the phase-shift oscillator with prescribed frequency and amplitude by using describing functions. Because oscillating condition varies with the operating points of the field-effect transistor, some discussion is included concerning reduction of this effect.

CHAPTER II

THEORETICAL ANALYSIS OF THE PHASE-SHIFT OSCILLATOR

A. Two Necessary Conditions for Oscillation

1. The active device furnishes power gain at the frequency of oscillation. This gain must be large enough to overcome circuit losses and establish exactly unity gain around the feedback loop.

2. The phase shifts introduced by the active device and the feedback network result in exactly zero phase shift around the overall circuit.

These conditions will permit sustained oscillation, but they do not guarantee that oscillation will occur. In other words, it is not enough that unity loop gain can exist. There must be more than unity loop gain at first to cause buildup of oscillations. These, then, are the necessary and sufficient conditions for the buildup and maintenance of self-sustained oscillation in a circuit.

B. Stability of RC Feedback System

The overall active circuit for the phase-shift oscillator is shown in Figure 2.

Any practical amplifier saturates if the magnitude of the signal voltage applied to it becomes sufficiently large. Accordingly, a nonlinear transmission characteristic is evident. This saturation effect can be considered by including a limiter following the "ideal"

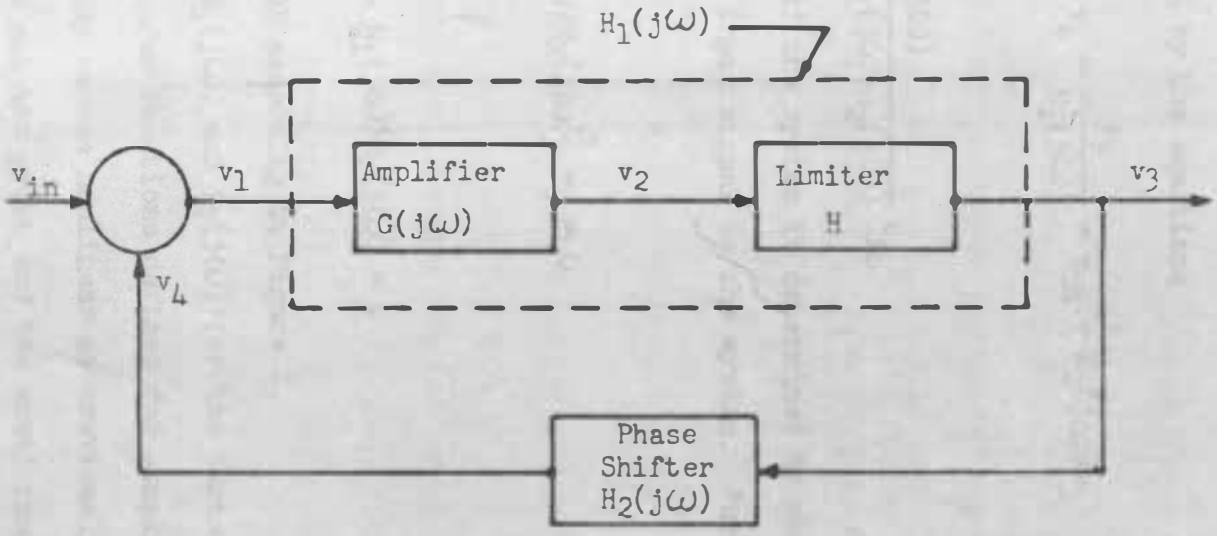

Figure 2. Block Diagram of Phase-Shift Oscillator

linear amplifier, as shown in Figure 2. The limiter may be left out or H can be set equal to unity for non-saturation conditions. In any case, the effects due to the limiting and the amplification will be represented by $H_1(j\omega)$. Including the phase shifter, the entire system can be analysed by the equations

$$v_1 = v_{in} + v_4 = \frac{v_3}{H_1(j\omega)} = v_{in} + H_2(j\omega)v_3$$

Then

$$v_3 = \frac{H_1(j\omega)}{1 - H_1(j\omega)H_2(j\omega)} v_{in} \qquad (1)$$

Asymptotic stability of the system is determined by what happens in the absence of any input signal to the system. For $v_{in} = 0$, Eq. (1) becomes

$$\left[1 - H_1(j\omega)H_2(j\omega)\right] v_3 = 0 \qquad (2)$$

We shall let

$$f(\lambda) = 1 - H_1(j\omega)H_2(j\omega) = 0 \qquad (3)$$

where $H_1(j\omega) = G(j\omega)H$ according to Figure 2.

The functions $H_1(j\omega)$ and $H_2(j\omega)$ for the parts of the system become merely the transfer functions defined for simple-harmonic variations. $H_1(j\omega)$ may become nonlinear as previously discussed. If the nonlinearity is not too great and the waveforms in the system are essentially sinusoidal in shape, the Nyquist criterion can be applied to test the stability of the system. If the system is such

that the waveforms depart considerably from a sinusoidal shape, testing the stability in this way may lead to erroneous conclusions.

By applying the Nyquist criterion, the stability of the system including the limiter is accordingly governed by the relation

$$1 - G(j\omega)HH_2(j\omega) = 0 \tag{4}$$

This is merely Eq. (3) with $H_1 = G(j\omega)H$, where H is the describing function for the limiter and is a function of the input amplitude. The value of H is real and positive; it will be discussed later. Eq. (4) can be put into more convenient form for study by writing it as

$$\frac{1}{G(j\omega)H_2(j\omega)} = H \tag{5}$$

This is the condition necessary for steady-state oscillation.

In analyzing a nonlinear system, it is convenient to write the relation for testing the stability as is done in Eq. (5). Those terms depending upon frequency appear on one side of the equation, and those depending upon amplitude appear on the opposite side.

Separation of this sort can be achieved where operation of the nonlinear element depends only upon amplitude of the signal, and that of the linear element depends only upon frequency. A more complicated situation arises if the nonlinear effect is also frequency dependent but this does not happen in the present case.

C. Describing Functions for the Limiter

A more intense investigation of the properties of the describing function for the limiter will be undertaken with the consideration of the transmission characteristic.

A nonlinearity can be described by a complicated equation which consists of the sum of separate simple-harmonic functions. In electronic applications, any periodic waveform can be expressed by a Fourier Series no matter how complicated the transmission characteristic is. If an input is $v_1 = V_1 \sin \omega t$, then the corresponding output v_3 in Figure 2 can be expressed as

$$v_3 = A_0 + A_1 \sin \omega t + B_1 \cos \omega t + \ldots + A_n \sin n\omega t + B_n \cos n\omega t + \ldots . \qquad (6)$$

If there are significant low-pass filtering and D.C. blocking effects, only fundamental components need be considered at oscillation because the signal fed back is almost purely sinusoidal. Therefore, Eq. (6) can be approximated by

$$v_3 \approx A_1 \sin \omega t + B_1 \cos \omega t \qquad (7)$$

Since $\cos \omega t$ is related to the first derivative of $\sin \omega t$, the physical meaning of Eq. (7) can be interpreted as follows: the output is a function of the input and its first derivative. Mathematically, this can be expressed by

$$v_3 = F(v_1, v_1') \qquad (8\text{-a})$$

$$= F_1(v_1) + F_2(v_1') \tag{8-b}$$

$$= g(V_1)v_1 + \frac{b(V_1)}{\omega} v_1' \tag{8-c}$$

$$= g(V_1)V_1 \sin \omega t + b(V_1)V_1 \cos \omega t \tag{8-d}$$

$$= A' \sin (\omega t + \phi) \tag{8-e}$$

Where V_1 is the peak amplitude of the input, v_1' is the first derivative of v_1, and

$$A' = V_1\sqrt{[g(V_1)]^2 + [b(V_1)]^2}\ , \quad \phi = \tan^{-1} \frac{b(V_1)}{g(V_1)} \tag{9}$$

For the condition given in Eq. (7), a hysteresis loop will exist on a plot of the transmission characteristic. The phase angle ϕ in Eq. (8-e) possesses a value other than the integral multiples of 180°. If the coefficient B_1 in Eq. (7) is zero, there is no hysteresis loop on the transmission characteristic. The phase angle ϕ in Eq. (8-e) is then an integral multiple of 180°. Eq. (8-e) is merely

$$v_3 = A \sin (\omega t + n\pi) \tag{10}$$

where $A = V_1 g(V_1)$ and $n = 0, 1, 2, \ldots$.

For most occasions, n equals unity because the phase shift between the input and the output is 180°.

D. Two Common Nonlinear Transmission Characteristics

One common multivalued nonlinearity is shown in Figure 3. The nonlinearity is not severe since the waveform of the output is essentially sinusoidal in shape. So, Eq. (8-d) is applicable.

The functions $g(V_1)$ and $b(V_1)$ are given by

$$g(V_1) = \frac{1}{\pi V_1}\int_0^{2\pi} F(v_1, v_1') \sin\theta \, d\theta$$
$$b(V_1) = \frac{1}{\pi V_1}\int_0^{2\pi} F(v_1, v_1') \cos\theta \, d\theta \qquad (11)$$

Here the input is taken to be $v_1 = V_1 \sin \omega t$ and the magnitude of the amplification or the absolute value of the slope of the transmission characteristic is taken to be $|G|$. Referring to Eqs. (10) and (11) in Appendix A, the nonlinear functions are derived as

$$g(V_1) = \frac{-|G|}{\pi}\left(\theta_2 + \theta_1 + \frac{\sin 2\theta_2}{2} + \frac{\sin 2\theta_1}{2}\right) \qquad (12)$$

$$b(V_1) = \frac{|G|}{\pi}\left(\sin^2\theta_2 - \sin^2\theta_1\right) \qquad (13)$$

where

$$\theta_1 = \sin^{-1}\frac{c - b|G|}{V_1|G|}, \quad \theta_2 = \sin^{-1}\frac{c + b|G|}{V_1|G|} \qquad (14)$$

From Eqs. (8), (12), and (13), the output is

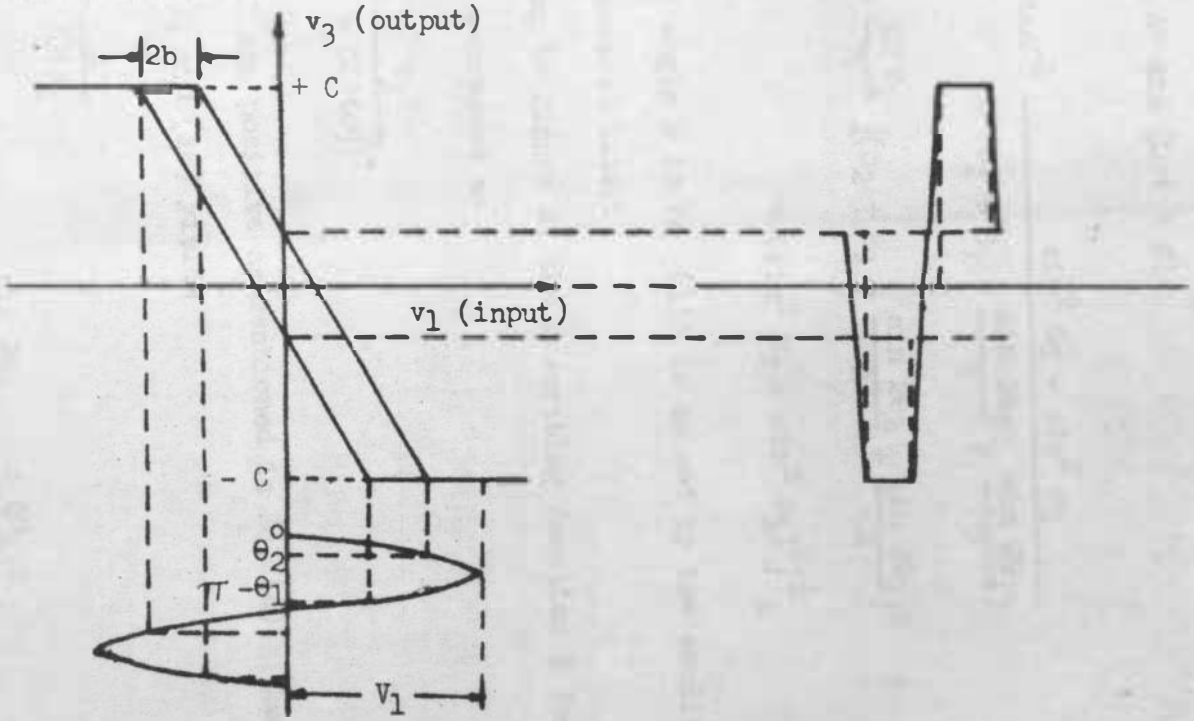

Figure 3. Transmission Characteristic with a Phase Shift a Little Smaller than 180°

$$v_3 \approx F_1(v_1) + F_2(v_1')$$

$$= g(V_1)V_1 \sin \omega t + b(V_1)V_1 \cos \omega t$$

$$= V_1 \left[g(V_1)\right]^2 + \left[b(V_1)\right]^2 \sin (\omega t + \phi)$$

$$= A' \sin (\omega t + \phi) \tag{15}$$

where
$$\phi = \tan^{-1} \frac{\sin^2 \theta_2 - \sin^2 \theta_1}{-(\theta_2 + \theta_1 + \frac{\sin 2\theta_2}{2} + \frac{\sin 2\theta_1}{2})} \tag{16}$$

and

$$A' = \frac{|G| V_1}{\pi} \left[(\theta_2 + \theta_1 + \frac{\sin 2\theta_2}{2} + \frac{\sin 2\theta_1}{2})^2 + (\sin^2 \theta_2 - \sin^2 \theta_1)^2\right]^{\frac{1}{2}} \tag{17}$$

The phase shift angle ϕ in Eq. (15) is caused by the amplification and will be discussed later.

Referring to Figure 2, the describing function H for the limiter can be expressed as

$$H = \frac{v_3}{v_1 G(j\omega)} \tag{18}$$

where H is real and positive as mentioned in Eq. (4). Combining Eqs. (15), (17), and (18) yields

$$H = \frac{A'}{|G| V_1}$$

$$= \frac{1}{\pi} \left[(\theta_2 + \theta_1 + \frac{\sin 2\theta_2}{2} + \frac{\sin 2\theta_1}{2})^2 + (\sin^2 \theta_2 - \sin^2 \theta_1)^2\right]^{\frac{1}{2}} \tag{19-a}$$

$$= \frac{1}{|G|}\sqrt{[g(V_1)]^2 + [b(V_1)]^2} \qquad (19\text{-b})$$

If the phase shift between the input and the output is an integral multiple of 180°, the transmission characteristic in Figure 3 will be single-valued, i.e., without hysteresis. Eqs. (12) and (13) will take another form with b = 0 and $\theta_1 = \theta_2$ in Figure 3.

$$g(V_1) = \frac{2|G|}{\pi}(\theta_1 + \sin\theta_1 \cos\theta_1) \qquad (20)$$

$$b(V_1) = 0 \qquad (21)$$

After substitution of Eqs. (20) and (21) into Eq. (8-c), the corresponding output* will be

$$v_3 = F_1(v_1)$$

$$= \frac{2GV_1}{\pi}(\theta_1 + \sin\theta_1 \cos\theta_1)\sin\omega t = A \sin(\omega t + n\pi) \qquad (22)$$

where $\theta_1 = \sin^{-1}\frac{V_c}{V_1}$ and V_c is the critical peak input amplitude at which the output starts to become saturated. As long as the input is smaller than V_c, the corresponding output will be

$$v_3 = GV_1 \sin\omega t \qquad (23)$$

---

*Note: $v_3 = |G|\left[1 - \frac{2}{\pi}(\theta_1 - \cos\theta_1 \sin\theta_1)\right]\cos(\omega t + n\pi)$ if the input is considered as $v_1 = V_1 \cos\omega t$.

The single-valued describing function for the limiter can be calculated from Eqs. (22) and (23):

$$H = 1 \qquad \text{if } V_1 \leq V_c \tag{24}$$

$$H = \frac{2}{\pi}(\theta_1 + \sin\theta_1 \cos\theta_1) \quad \text{if } V_1 \geq V_c \tag{25}$$

Comparison between Eq. (15) and Eq. (22) reveals that there is no fundamental cosine term in Eq. (22) since the phase shift angle n determines only the positive or negative value of the peak amplitude. Therefore, the output is a function of only its input as long as the single-valued transmission characteristic is concerned.

Another multivalued nonlinearity is shown in Figure 4. This might be called partial saturation. The "quasilinear" analytic method is still an effective tool to analyze this problem.

The phrase, "partial saturation", refers to the transmission characteristic with either saturation or cut-off. It is the operating point of the active device that makes this case different from the full saturation case.

Referring to Eqs. (25) and (26) in Appendix B, the functions are derived as follows:

$$g(V_1) = \frac{-|G|}{2}\left[\frac{\pi}{2} + (\theta_1 + \theta_2 + \theta_3) + \sin\theta_1 \cos\theta_1 + (1 - \sin\theta_1)(\cos\theta_2 - \cos\theta_3) + \sin(\theta_2 + \theta_3)\right] \tag{26}$$

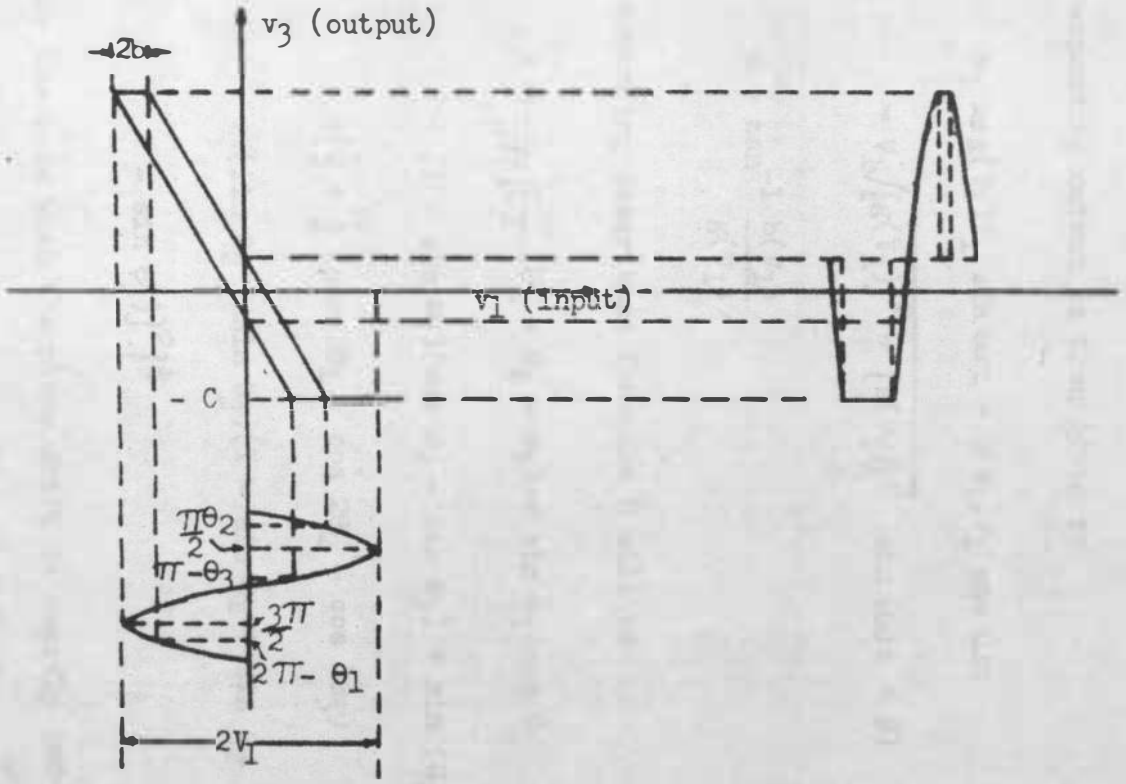

Figure 4. Partial Saturation Transmission Characteristic with a Phase Shift a Little Smaller than 180°

$$b(V_1) = \frac{|G|}{2\pi}\left[\frac{1}{2} + \frac{1}{2}(\cos 2\theta_1 + \cos 2\theta_2 - \cos 2\theta_3) + (\sin \theta_2 + \sin \theta_2)(1 - \sin \theta_1 + \sin \theta_2 - \sin \theta_3)\right] \quad (27)$$

The corresponding output is then given by

$$v_3 \approx g(V_1)V_1 \sin \omega t + b(V_1)V_1 \cos \omega t = V_1\sqrt{[g(V_1)]^2 + [b(V_1)]^2} \sin(\omega t + \phi) \quad (28\text{-a})$$

where

$$\phi = \tan^{-1} \frac{b(V_1)}{g(V_1)} \quad (28\text{-b})$$

The corresponding describing function H will be

$$H = \frac{1}{2\pi}\left\{\left[\frac{\pi}{2}(\theta_1 + \theta_2 + \theta_3) + \sin \theta_1 \cos \theta_1 + (1 - \sin \theta_1)(\cos \theta_2 - \cos \theta_3) + \sin(\theta_2 + \theta_3)\right]^2 + \left[\frac{1}{2} + \frac{1}{2}(\cos 2\theta_1 + \cos 2\theta_2 - \cos 2\theta_3) + (\sin \theta_2 + \sin \theta_3)(1 - \sin \theta_1 + \sin \theta_2 - \sin \theta_3)\right]^2\right\}^{\frac{1}{2}} \quad (29)$$

For the case when the phase shift is exactly 180°, the hysteresis in Figure 4 disappears; hence $b = 0$, $\theta_1 = \frac{\pi}{2}$, and $\theta_2 = \theta_3$. Eqs. (26), (27), and (29) will reduce to simpler forms as follows:

$$g(V_1) = -|G|\left[\frac{1}{2} + \frac{1}{\pi}(\theta_2 + \sin\theta_2 \cos\theta_2)\right] \tag{30}$$

$$b(V_1) = 0 \tag{31}$$

$$v_3 = GV_1\left[\frac{1}{2} + \frac{1}{\pi}(\theta_2 + \sin\theta_2 \cos\theta_2)\right] \sin\omega t \tag{32}$$

Therefore

$$H = 1 \qquad \text{if } V_1 \leq V_c \tag{33-a}$$

$$H = \frac{1}{2} + \frac{1}{\pi}(\theta_2 + \sin\theta_2 \cos\theta_2) \qquad \text{if } V_1 \geq V_c \tag{33-b}$$

where V_c is the critical peak input voltage at which the partial saturation starts.

E. Analysis of FET at Low Frequency

So far the behavior of the limiter has been discussed. Eq. (5) reveals that the analyses of the amplifier and the phase shifters are necessary in order to understand the conditions for steady-state oscillation.

At low frequencies, the equivalent circuit of the field-effect transistor is essentially as shown in Figure 5.

The resistances of r_{dg} and r_{gs} are usually large enough so that they may be neglected. The voltage gain of the amplifier is

$$G = -\, g_m \frac{r_{ds}\, Z_\ell}{r_{ds} + Z_\ell} \tag{34}$$

where g_m is the transconductance of the FET.

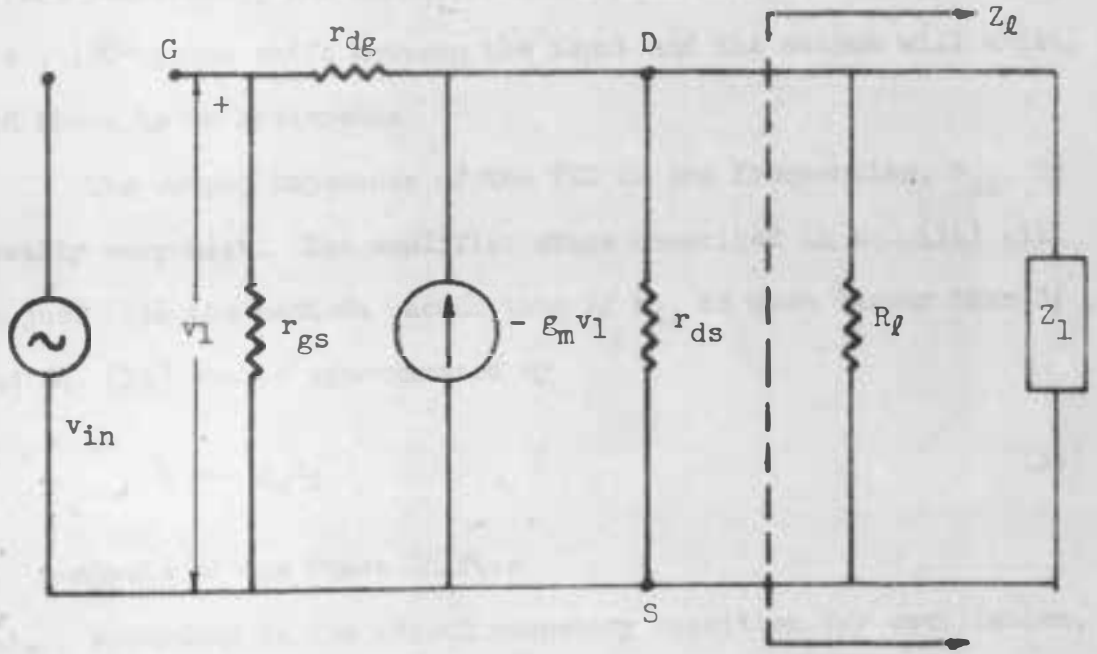

Figure 5. Low Frequency FET Equivalent Circuit with Load Z_ℓ and Source v_{in}

The amplification G will be a real negative number if Z_ℓ is real. When the load Z_ℓ is not a pure resistance, the corresponding complex amplification G will cause a hysteresis loop on the transmission characteristic plot. The phase shift between the input and the output will be other than 180°. If the load Z_ℓ is a pure resistance, the amplification G will have a negative value, i.e., 180° phase shift between the input and the output will exist, and there is no hysteresis.

The output impedance of the FET at low frequencies, r_{ds}, is usually very high. The amplifier stage described in Eq. (34) will be just like the pentode vacuum tube if r_{ds} is much larger than Z_ℓ, and Eq. (34) can be approximated by

$$G = - g_m Z_\ell \tag{35}$$

F. Analysis of the Phase Shifter

According to the second necessary condition for oscillation, the phase shift caused by the amplifier must be added to that of the phase shifter. A variety of phase shifting networks may be employed with oscillators. One often used is shown in Figure 6. It consists of a ladder composed of three equal resistances R and three equal capacitances C.

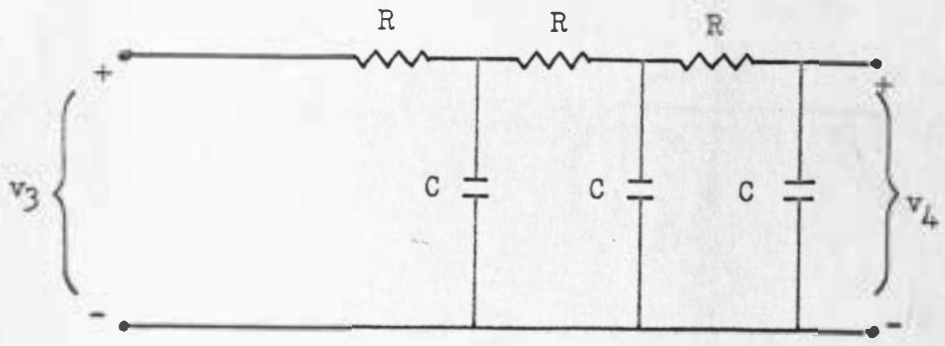

Figure 6. Low-pass RC Phase Shifter

The transfer function for this network is

$$H_2(j\omega) = \frac{v_4}{v_3} = \frac{1}{(jRC\omega)^3 + 5(jRC\omega)^2 + 6(jRC\omega) + 1} \qquad (36)$$

The reciprocal of Eq. (36) is

$$\frac{1}{H_2(j\omega)} = (jRC\omega)^3 + 5(jRC\omega)^2 + 6(jRC\omega) + 1 \qquad (37)$$

Eq. (37) is plotted in Figure 7. Substitution of Eqs. (35) and (37) into Eq. (5) yields

$$\frac{(jRC\omega)^3 + 5(jRC\omega)^2 + 6(jRC\omega) + 1}{-g_m Z_\ell} \qquad (38)$$

Eq. (38) states the condition for steady-state oscillation.

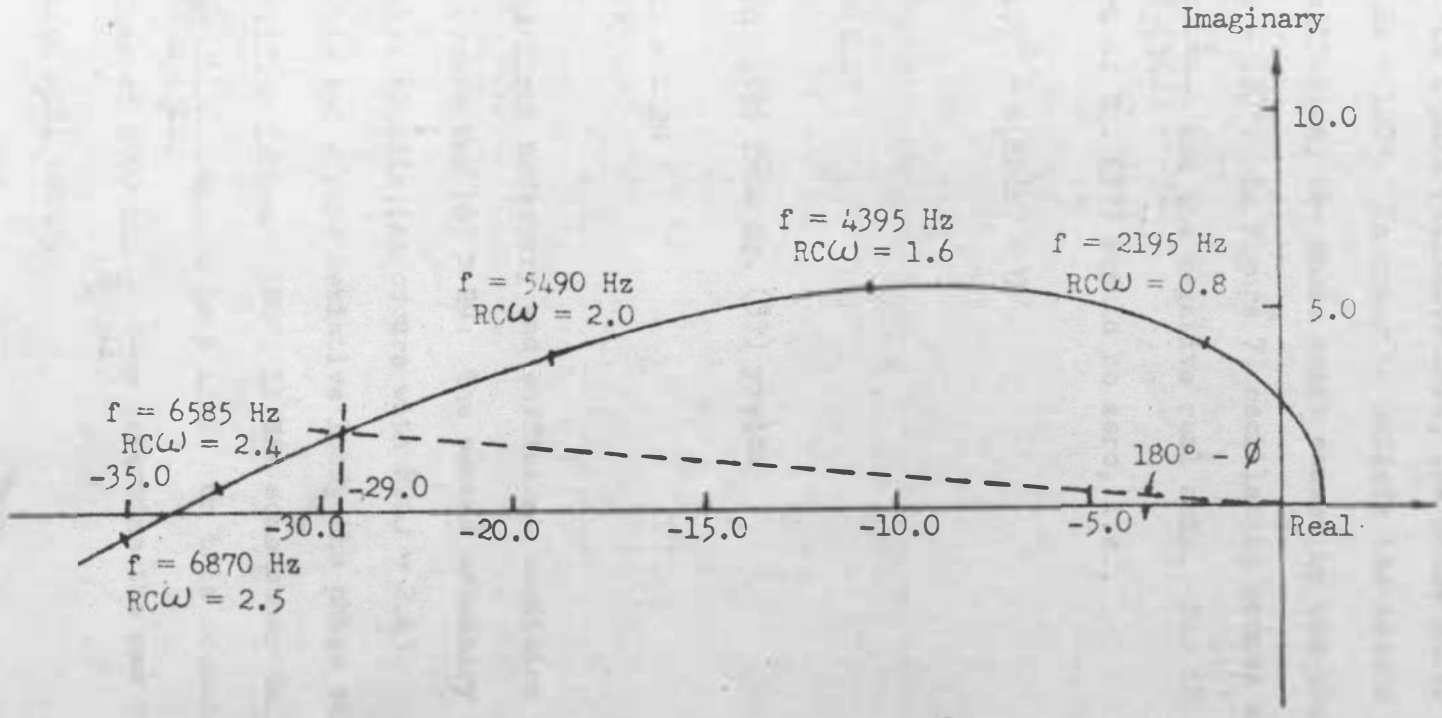

Figure 7. Circuit Loss of the Phase Shifter of Figure 6

G. Oscillator Considerations

1. If Z_L is a pure resistive load, the phase shift caused by the amplifier is + 180°. In order to satisfy the second necessary condition for oscillation, the phase shift caused by the phase shifter should be - 180°. In Figure 7, oscillation occurs at the intersection of $\frac{1}{H_2(j\omega)}$ and the negative real axis. For this case, the imaginary part of Eq. (37) should be zero, i.e.,

$$-(RC\omega)^3 + 6(RC\omega) = 0$$

or

$$RC\omega = 2.45 \tag{39}$$

Substitution of Eq. (39) into Eq. (37) yields

$$\frac{1}{H_2(j\omega)} = -29 \tag{40}$$

In all, the first necessary and sufficient condition predicts that oscillation occurs for $|G| > 29$. The second necessary condition predicts that oscillation occurs with $RC\omega = 2.45$.

2. If Z_L is not a pure resistive load, the phase shift caused by the amplifier is not + 180°; it has some other value ϕ. The phase angle of $\frac{1}{H_2(j\omega)}$ should be ϕ also. On this occasion, the corresponding values of $RC\omega$ and $\frac{1}{H_2(j\omega)}$ determine the new condition at which oscillation will occur.

3. From Item 1 and Item 2, the left side of Equation (38) should result in a real and positive value at oscillation. Therefore H is a real and positive value as mentioned in Eqs. (4) and (18). Furthermore, the sufficient condition for oscillation states that amplification G should be larger than the circuit loss $\frac{1}{H_2(j\omega)}$. So

$$H = \left| \frac{1}{G(j\omega)H_2(j\omega)} \right| < 1 \qquad (41)$$

Eq. (41) states that oscillation of this kind is always saturated.

CHAPTER III

THE FET PHASE SHIFT OSCILLATOR

A. Analysis of a Practical FET Oscillator

The practical oscillator circuit is shown in Figure 8. Nominal values are

$R = 50\ k\Omega$ $\qquad C = 1160\ pf$

$R_L = 20\ k\Omega$ $\qquad C_1 = 0.35\ \mu f$

$R_g = 1\ M\Omega$

In the first investigation, the effects of the elements R_g and C_1 are neglected.

$$Z_1 = R + \cfrac{1}{SC + \cfrac{1}{R + \cfrac{1}{SC + \cfrac{1}{R + \cfrac{1}{SC}}}}} = \frac{R^3C^3S^3 + 5R^2C^2S^2 + 6RCS + 1}{R^2C^3S^3 + 4RC^2S^2 + 3CS} \tag{42}$$

$$= \frac{(R^5C^6\omega^6 + 23R^3C^4\omega^4 + 14RC^2\omega^2) - j(R^4C^5\omega^5 + 8R^2C^3\omega^3 + 3C\omega)}{16R^2C^4\omega^4 + (R^2C^3\omega^3 - 3C\omega)^2}$$

From Eq. (42) it is apparent that $I_m[Z_1] \neq 0$ except when $\omega = 0$. Therefore the resultant load on the FET stage is always a complex impedance.

Let $Z_1 = R_1 - jX_1$, then

$$Z = \frac{R_\ell'(R_1 - jX_1)}{(R_\ell' + R_1) - jX_1} = \frac{R_\ell' \, |Z_1|}{|Z_d|} \angle -\alpha + \beta \qquad (43)$$

where R_ℓ' equals $\frac{R_\ell r_{ds}}{R_\ell + r_{ds}}$ and r_{ds} is the output impedance of the FET as shown in Figure 5. Figure 9 is used to explain Eq. (43). The phase angle of the resultant load impedance Z_ℓ is $-\psi$. From Figure 9 it is clear that a smaller load resistance R_ℓ will cause a smaller resultant negative phase angle, $-\psi$, for the total load impedance Z_ℓ . Referring to Figure 5, an understanding of the effect upon oscillation at various operating points is available. The output impedance of the FET, r_{ds}, is usually very high but by no means infinite. The value of r_{ds} varies with operating point and it is essentially in parallel with R_ℓ . Therefore, a different effective load resistor R_ℓ' will result. According to Figure 9, the different resultant negative phase angle of the total load impedance Z_ℓ due to the effective load resistor R_ℓ' will affect the oscillation conditions, although all elements of the phase shifter are kept the same. It will be observed that the frequency of oscillation changes with operating point. An operating point at which a lower r_{ds} is apparent provides a correspondingly higher oscillation frequency. Fortunately, r_{ds} is often considerably

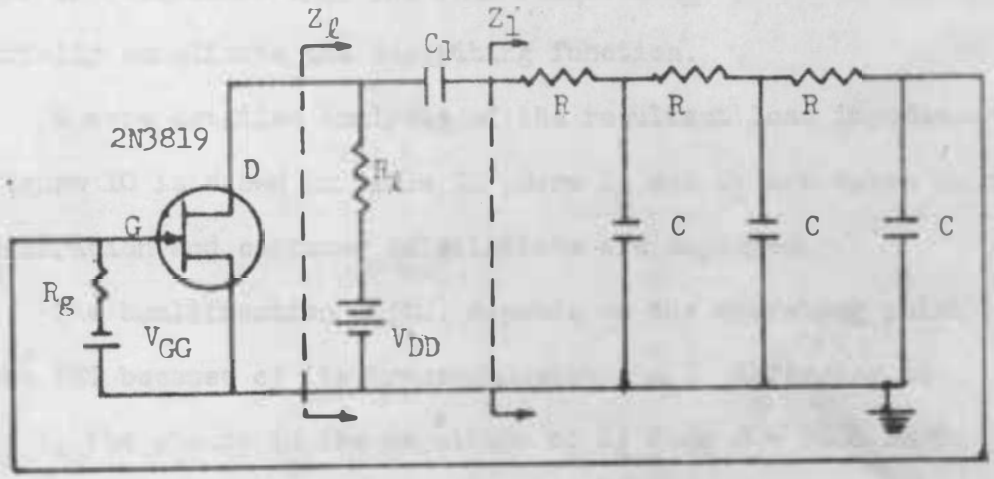

Figure 8. Designed RC Phase-Shift Oscillator

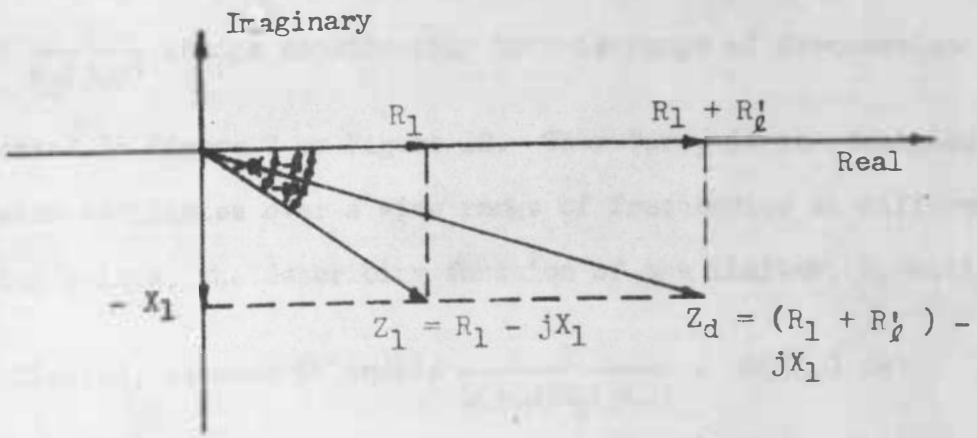

Figure 9. Phase Angle of the Equivalent Load in Figure 5.

higher in resistance than the load resistor R_ℓ and it does not materially complicate the describing function.

A more detailed analysis of the resultant load impedance Z_ℓ in Figure 10 is shown in Table I. Here R_g and C_1 are taken into consideration and computer calculations are employed.

The amplification $G(j\omega)$ depends on the operating point of the FET because of its transconductance g_m. Referring to Table I, the change in the magnitude of Z_ℓ from f = 6000 Hz to f = 7000 Hz is less than 1% and the change of the corresponding phase angle is 0.29°. Since the amplification $G(j\omega)$ equals approximately $- g_m Z_\ell$ at low frequencies, there is negligible change in the amplification $G(j\omega)$ in this range of frequencies at a particular operating point. However, both the magnitude and the phase angle of the feedback coefficient $H_2(j\omega)$ or the loss of the circuit $\frac{1}{H_2(j\omega)}$ change considerably in this range of frequencies as observed in Figure 7 or Figure 12. Therefore, if the designed oscillator oscillates over a wide range of frequencies at different operating points, the describing function of the limiter, H, will be complicated, because it equals $\frac{1}{G(j\omega)H_2(j\omega)}$. $G(j\omega)$ is dependent on operating point but not frequency, whereas $H_2(j\omega)$ is dependent on frequency but not on operating point. If the designed oscillator oscillates over a narrow range of frequencies at different

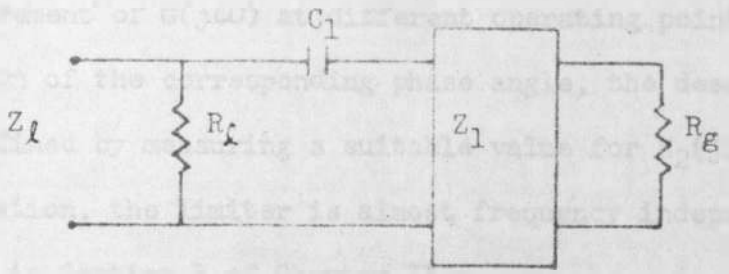

Figure 10. Load Appearing to the FET in Figure 8

TABLE I

Load Impedance Z_ℓ in the Frequency Range from 6000 Hz to 7000 Hz

Frequency f (Hz)	Impedance Z_ℓ (Ohms)	Phase Angle (degrees)
6000	1.5086×10^4	-4.58
6100	1.5071×10^4	-4.55
6200	1.5056×10^4	-4.52
6300	1.5042×10^4	-4.49
6400	1.5028×10^4	-4.46
6500	1.5014×10^4	-4.43
6600	1.5000×10^4	-4.40
6700	1.4987×10^4	-4.38
6800	1.4975×10^4	-4.35
6900	1.4962×10^4	-4.32
7000	1.4950×10^4	-4.29

operating points, $H_2(j\omega)$ will not complicate the problem. From the measurement of $G(j\omega)$ at different operating points and the calculation of the corresponding phase angle, the describing function can be defined by measuring a suitable value for $H_2(j\omega)$. Under this situation, the limiter is almost frequency independent as discussed in Section B of Chapter II.

If the load on the FET in Figure 10 were purely resistive and C_1 and R_g have no effect on the circuit, then the oscillation would occur at $RC\omega = 2.45$, i.e., $f = 6720$ Hz. But at $f = 6720$ Hz, the actual load is $Z_\ell = |Z_\ell| \angle -4.37°$ as shown in Table I. Using Eq. (35) to predict the amplification $G(j\omega)$ at this frequency yields

$$G(j\omega) = -g_m Z_\ell = g_m |Z_\ell| \angle 180° - \psi$$

$$= g_m |Z_\ell| \angle 180° - 4.37°$$

$$= g_m |Z_\ell| \angle 175.63° \qquad (44)$$

Therefore

$$\phi = 175.63°$$

where ϕ is the phase shift angle between the input and the output.

Now consider the second necessary condition for oscillation. For ϕ, as noted above, oscillation should occur at $RC\omega' = 2.24$ or $f' = 6150$ Hz according to Figure 7. This is the first correction to the designed value. At $f' = 6150$ Hz,

$$G'(j\omega) = g_m|Z_\ell'| \angle 180° - 4.54°$$

$$= g_m|Z_\ell'| \angle 175.46° \qquad (45)$$

Thus

$$\phi' = 175.46°$$

The second prediction of oscillation results in $RC\omega'' = 2.26$ or $f'' = 6210$ Hz. There is some discrepancy between the first and the second predictions. If we keep on correcting in this way, the final constant value will approach $RC\omega_m = 2.28$ or $f_m = 6250$ Hz accordingly. This reveals that the circuit will oscillate at $RC\omega = 2.28$ rather than $RC\omega = 2.45$. Therefore, if an oscillation frequency 6720 Hz is desired, the new value of the capacitive elements C_n should be

$$C_n = \frac{2.28}{2\pi \times 6720} = 1085 \text{ pf}$$

rather than C = 1160 pf, as previously used.

The contribution of impedance by any capacitor C at an angular velocity ω is $\frac{1}{jC\omega}$. It is worthy of mention to note that the correction of the capacitors does not affect the amplification $G(j\omega)$ at oscillation because of $RC\omega = RC_n\omega_n$. That is: the contribution to the impedance of the new capacitors at new oscillation frequency is the same as that of the old ones at old oscillation frequency.

B. Analysis of the Designed Phase Shifter

A detailed analysis of the phase shifter was made and shown in Figure 11. The method used employs computer calculations. The results of these computations are plotted in Figure 12.

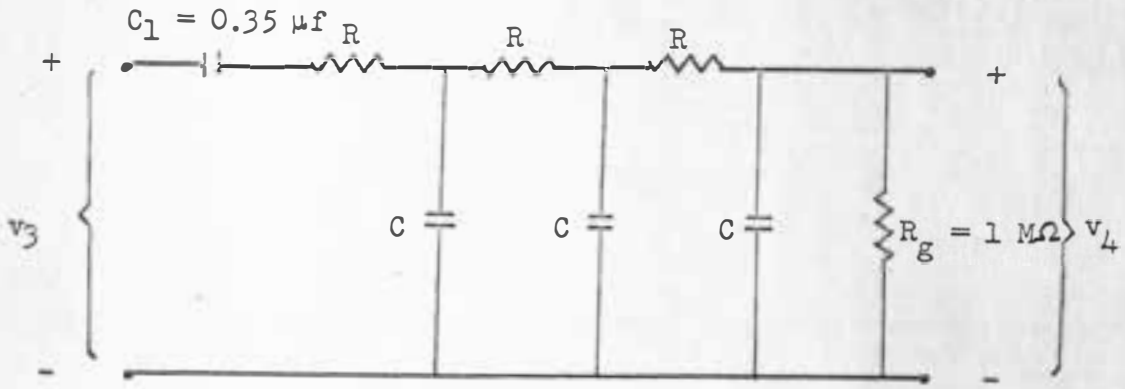

Figure 11. Effective Phase Shifter for the Designed Oscillator

After taking R_g and C_1 into consideration, the loss of the phase shifter shown in Figure 12 is larger than that in Figure 7. At 180°, it is 30.2 rather than 29.

C. Analysis of the Limiter

The complexity of Eqs. (19-a) and (29) for limiter describing functions is unfortunate. However, if the phase angle of the load impedance, Z_l , is smaller than 10°, the omission of $b(V_1)$ in Eqs. (19-a) and (29) will cause little error.

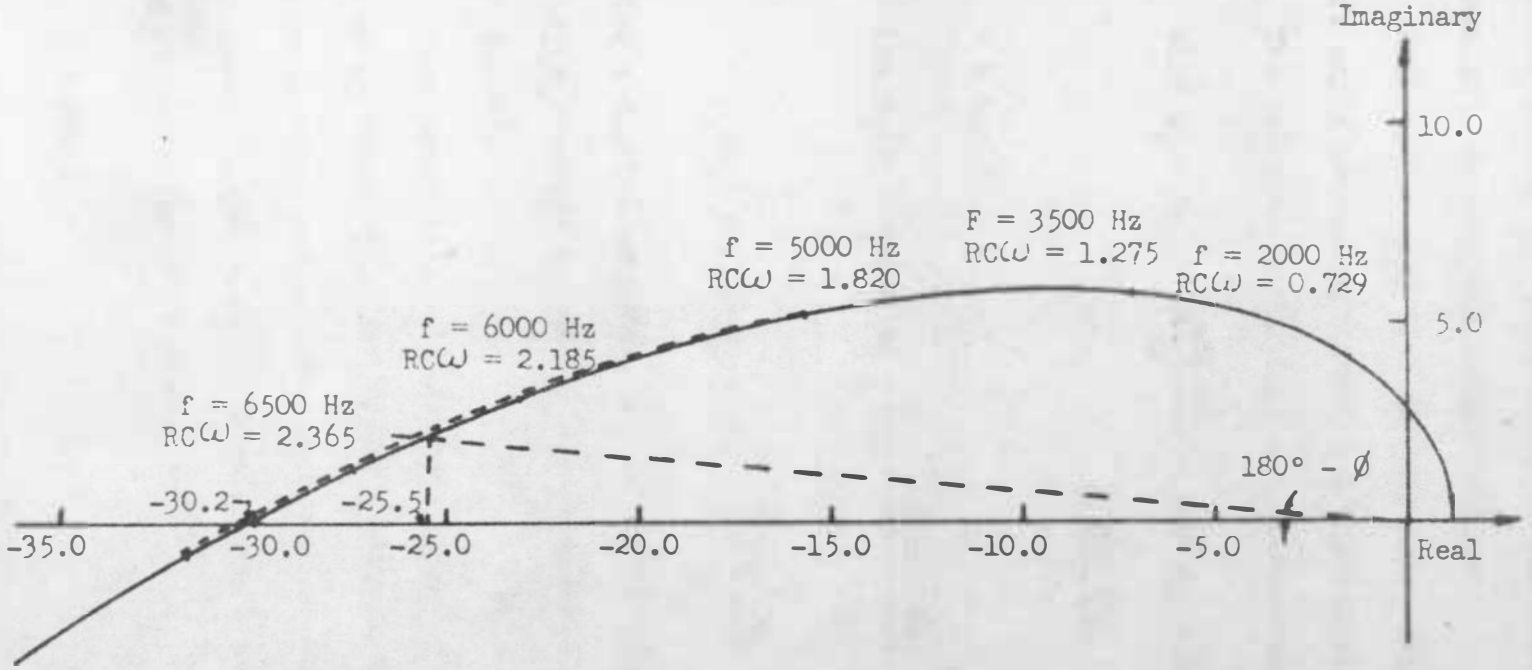

Figure 12. Detailed Analysis of the Circuit Loss of the Designed Phase Shifter in Figure 11

For the case of the phase angle of the load impedance Z_ℓ greater than 10°, an analysis method follows:

1. Analyze the amplifier and the phase shifter to get the phase shift angle between the input and the output.

2. The relation in Eq. (46) can be derived from Eq. (16)

$$\sin^2 \theta_1 - K\theta_1 - \frac{K \sin 2\theta_1}{2} = \sin^2 \theta_2 + K\theta_2 + \frac{K \sin 2\theta_2}{2} \tag{46}$$

where $K = \tan \phi$

3. Let $f_1(\theta_1) = \sin^2 \theta_1 - K\theta_1 - \frac{K \sin 2\theta_1}{2}$ (47)

and

$$f_2(\theta_2) = \sin^2 \theta_2 + K\theta_2 + \frac{K \sin 2\theta_2}{2} \tag{48}$$

By employing a digital computer, values may be obtained to plot curves of $f_1(\theta_1)$ versus θ_1, and $f_2(\theta_2)$ versus θ_2, by varying θ_1 and θ_2 from 0° to 90°.

4. Take pairs of points at which $f_1(\theta_1) = f_2(\theta_2)$ to plot the curve of θ_2 versus θ_1. By finite difference method or least squares approximation method, the relation $\theta_2 = f_3(\theta_1)$ can be found.

5. Substitute $\theta_2 = f_3(\theta_1)$ into Eq. (19) and get a simplified describing function for the limiter, thus

$$H = H(\theta_1) \tag{49}$$

6. If the relationship of the ratio $\frac{V_1}{V_c}$ and θ_1, can be defined from experimental data, then Eq. (49) can be replaced by

$$H = H(\frac{V_1}{V_c}) \tag{50}$$

Eq. (50) will lead to the solution of the problem.

For partial saturation case, the analytical method is still the same, but one more condition is necessary because there are three independent variables in Eq. (29), i.e., θ_1, θ_2, and θ_3. This additional condition can be obtained from Eq. (22) in Appendix B. From Eq. (22) in Appendix B and Eqs. (28-b) and (29) a new describing function in terms of $\frac{V_1}{V_c}$ can be derived by following the same procedures outlined above.

From the analyses of the previously discussed amplifier and the phase shifter, the oscillation will occur at $RC\omega = 2.28$ or $f = 6250$ Hz rather than at $RC\omega = 2.45$ or $f = 6720$ Hz. Refer to Table I: the phase angle ψ of the load impedance Z_ℓ is - 4.5° at $f = 6250$ Hz. The corresponding amplification $G(j\omega)$ should be

$$G(j\omega) = g_m |Z_\ell| \angle 180° - 4°30'$$

$$= g_m |Z_\ell| \angle 175°30' \tag{51}$$

or the phase shift angle of the amplifier $\phi = 175°30'$. Substitution of this into Eq. (9) yields

$$\frac{b(V_1)}{g(V_1)} = \tan^{-1} 175°30' = - 0.0785$$

or

$$b(V_1) = -0.0785\, g(V_1) \tag{52}$$

From Eqs. (19), (28), and (50)

$$H = \frac{1}{|G|}\sqrt{[g(V_1)]^2 + [b(V_1)]^2} = \frac{1}{|G|}\sqrt{[g(V_1)]^2 + 0.0064\,[g(V_1)]^2}$$

$$= \frac{1.003}{|G|}|g(V_1)| \approx \left|\frac{g(V_1)}{G}\right| \tag{53}$$

Eq. (53) indicates that neglecting the phase shift in calculating the describing function for the limiter in the present example does not cause a significant error. Therefore, the prediction of the oscillation amplitudes by using Eqs. (25) and (33) should be satisfactory. Figure 13 shows the relationship of the limiter and the input voltage for the full saturation and partial saturation cases. For the full saturation case, as curve A shows, if $V_1 \leq V_c$, then $\theta_1 = \frac{\pi}{2}$ in Eq. (25) and H = 1. If $V_1 \gg V_c$ then $\theta_1 \rightarrow 0$ and $H \rightarrow \frac{4V_c}{\pi}$ as shown in Eq. (14-c) in Appendix A. For the partial saturation case, as curve B shows, if $V_1 \leq V_c$, then $\theta_2 = \frac{\pi}{2}$ in Eq. (33) and H = 1. For the partial saturation case, V_1 is never much larger than V_c as discussed at the end of Appendix B.

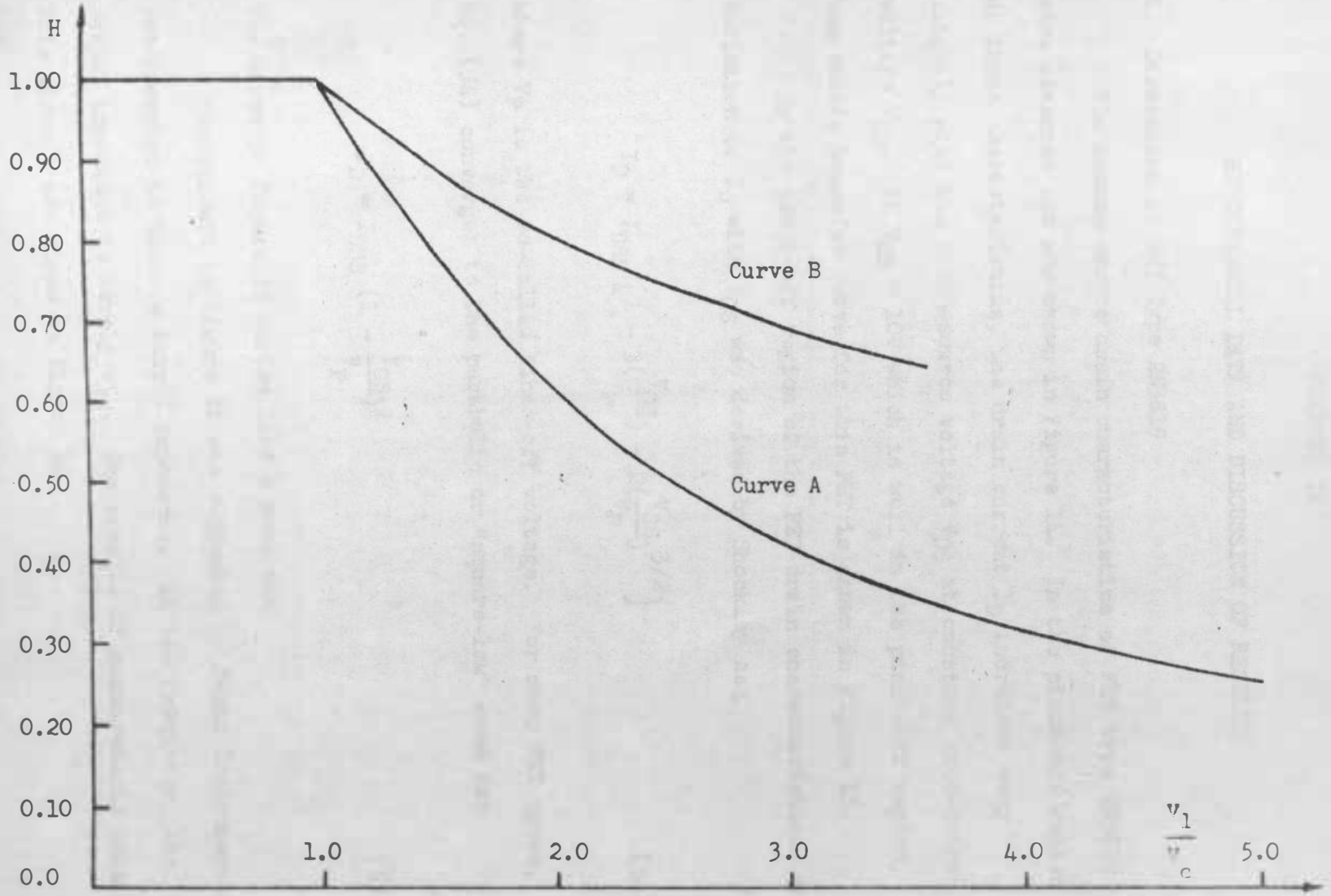

Figure 13. Nonlinear Describing Functions of Eqs. (20) and (33)

CHAPTER IV

EXPERIMENTAL DATA AND DISCUSSION OF RESULTS

A. Discussion of FET Type 2N3819

The common-source drain characteristics of FET type 2N3819 were measured and are shown in Figure 14. In the pinch-off region of these characteristics, the drain current I_D increases very slightly with the drain-source voltage V_{DS} at constant gate-source voltage V_{GS}. At V_{DS} = 10V which is well in the pinch-off region, the static transfer curve for this FET is shown in Figure 15.

In the pinch-off region of the FET drain characteristics, the variation of I_D with V_{GS} was derived by Shockley as:

$$I_D = I_{DSS}\left[1 - 3\left(\frac{V_{GS}}{V_P}\right) + 2\left(\frac{V_{GS}}{V_P}\right)^{3/2}\right] \tag{54}$$

where V_P is the so-called pinch-off voltage. For most FET types, Eq. (54) converges to the parabolic or "square-law" case as:

$$I_D = I_{DSS}\left(1 - \frac{V_{GS})^2}{V_P}\right. \tag{55}$$

The curve in Figure 15 varies like a parabola.

The circuit in Figure 16 was suggested by Texas Instruments Incorporated to measure output impedance. At low frequency, the output impedance is merely r_{ds}. The results of measurements using this circuit are shown in Figure 18.

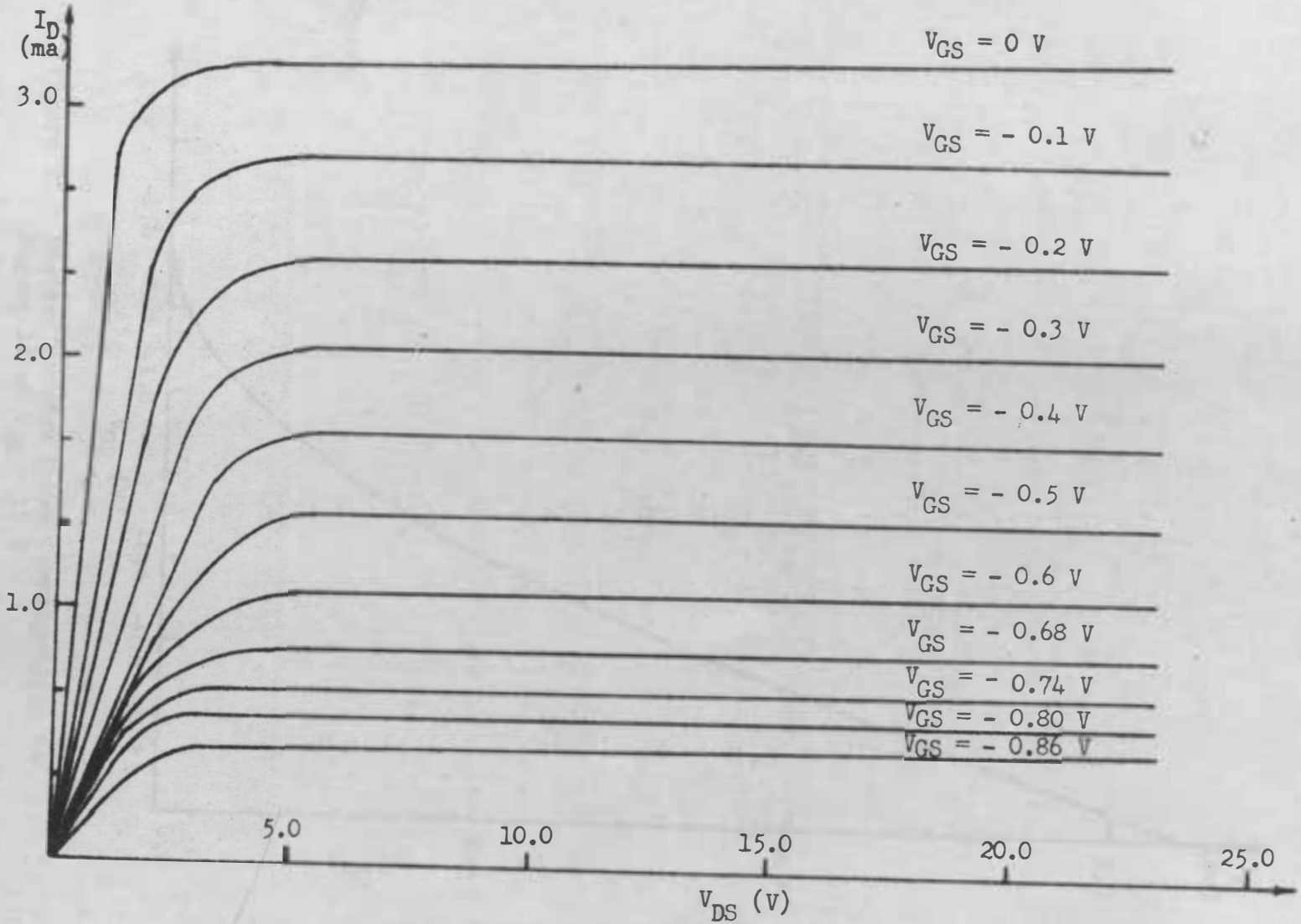

Figure 14. Drain Characteristic of FET Type 2N3819

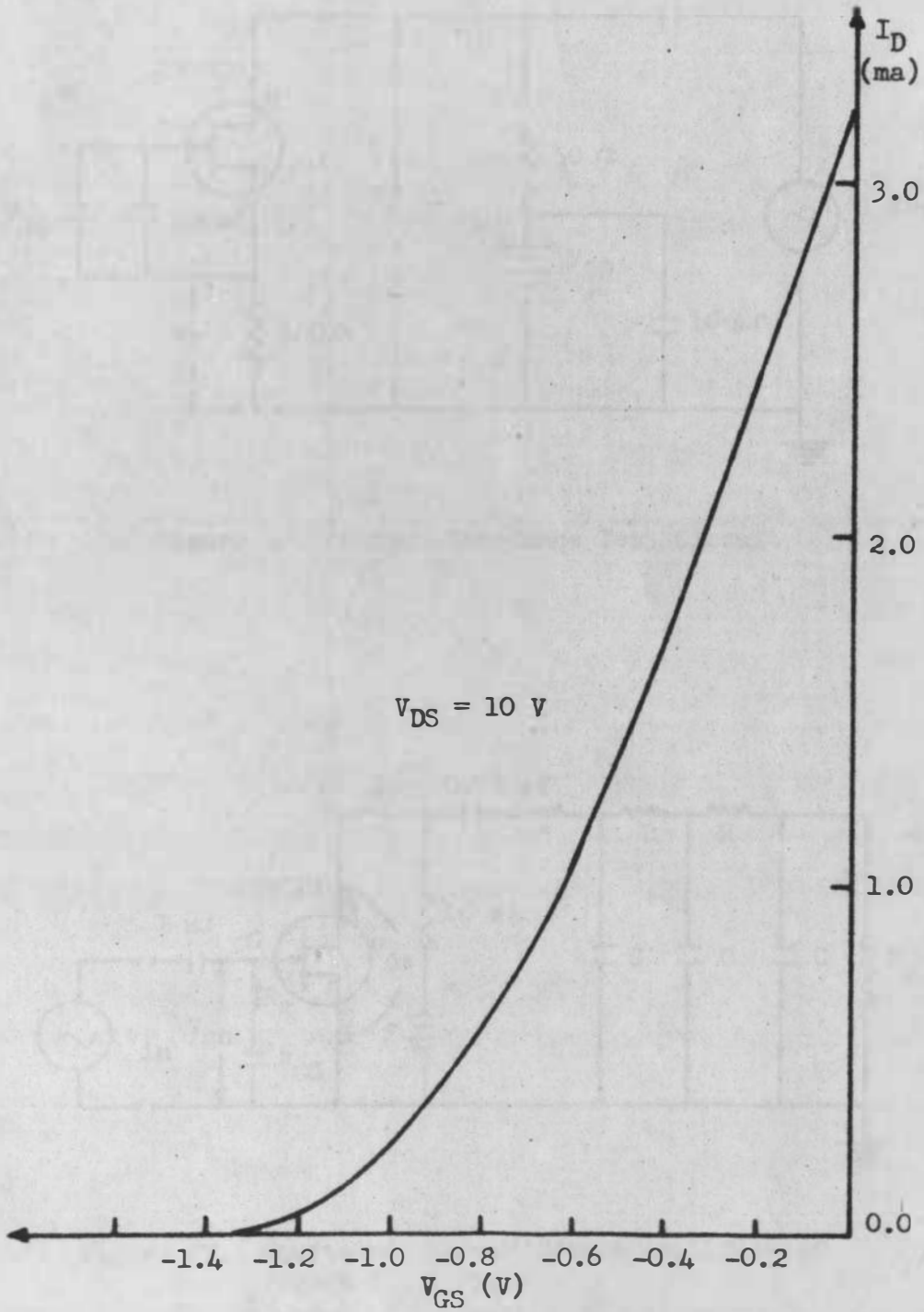

Figure 15. Static Transfer Curve Corresponding to Figure 14 at V_{DS} = 10 V

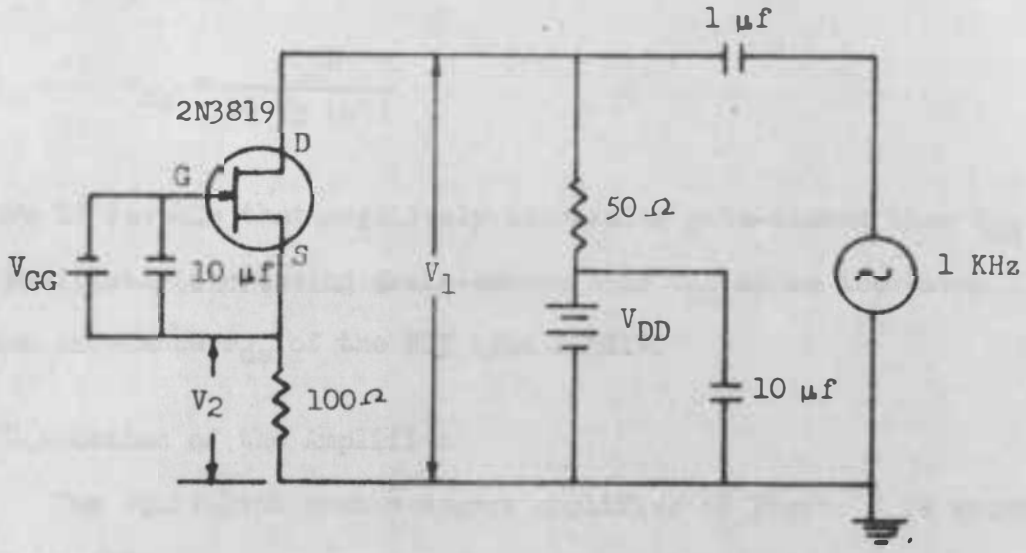

Figure 16. Output Impedance Test Circuit

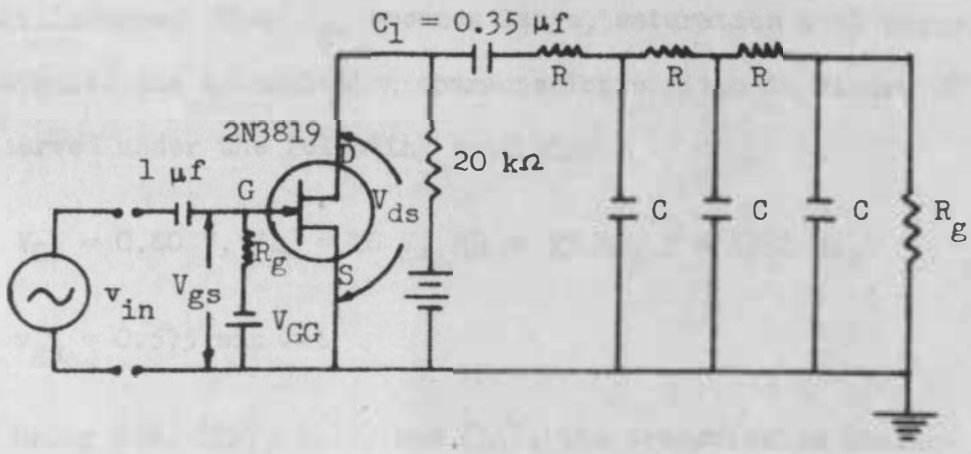

Figure 17. Equivalent Common-Source Amplifier of Figure 8

If $V_1 = 1$ V, then

$$r_{ds} = \frac{10^6}{10\ V_2\ (mV)}$$

Figure 18 reveals that negatively increasing gate-source bias V_{GS} and positively increasing drain-source bias V_{DS} cause increased output impedance r_{ds} of the FET type 2N3819.

B. Discussion of the Amplifier

The equivalent common-source amplifier of Figure 8 is shown in Figure 17.

The magnitude of the small-signal amplification of this amplifier stage at f = 6250 Hz is shown in Figure 19. The input signal v_{gs} was 0.003 V rms. The hysteresis loop associated with the transmission characteristic can be easily observed with type 503 oscilloscope. When v_{gs} becomes large, saturation will occur. For instance, the transmission characteristic given in Figure 20 was observed under the following conditions:

$$V_{GS} = 0.80\ V,\ V_{DS} = 16\ V,\ |G| = 33.85,\ f = 6250\ Hz,$$

$$v_{gs} = 0.575 \sin \omega t$$

Using Eqs. (12), (13), and (14), the transmission characteristic in Figure 20 can be analyzed approximately as follows:

$$\theta_1 = \sin^{-1} \frac{c - b|G|}{V_1\ |G|} = \sin^{-1} \frac{14 - 0.04 \times 33.85}{0.575 \times 33.85} = 0.707$$

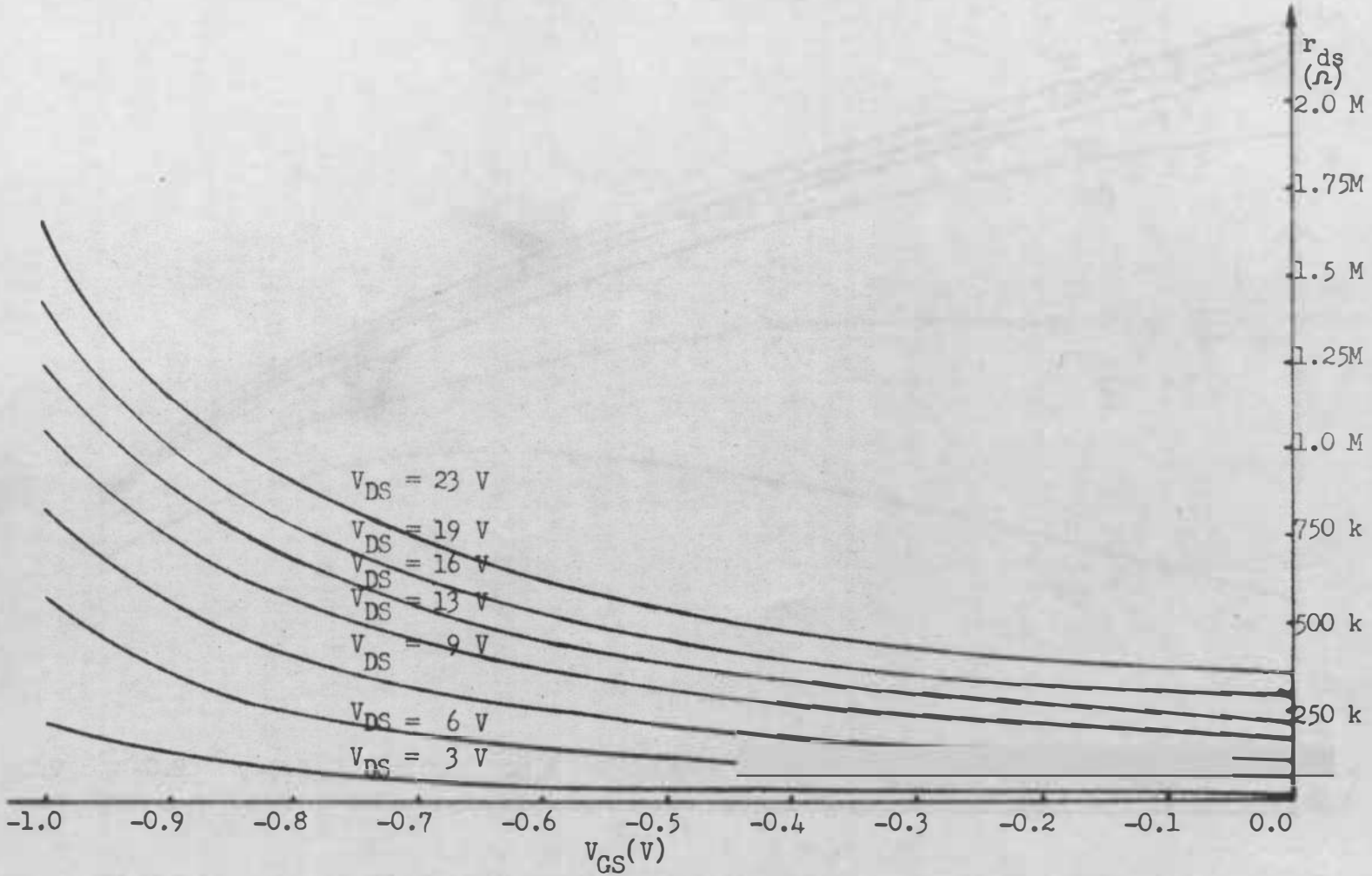

Figure 18. Output Impedance r_{ds} of FET Type 2N3819 at Various Operating Points at Low Frequencies

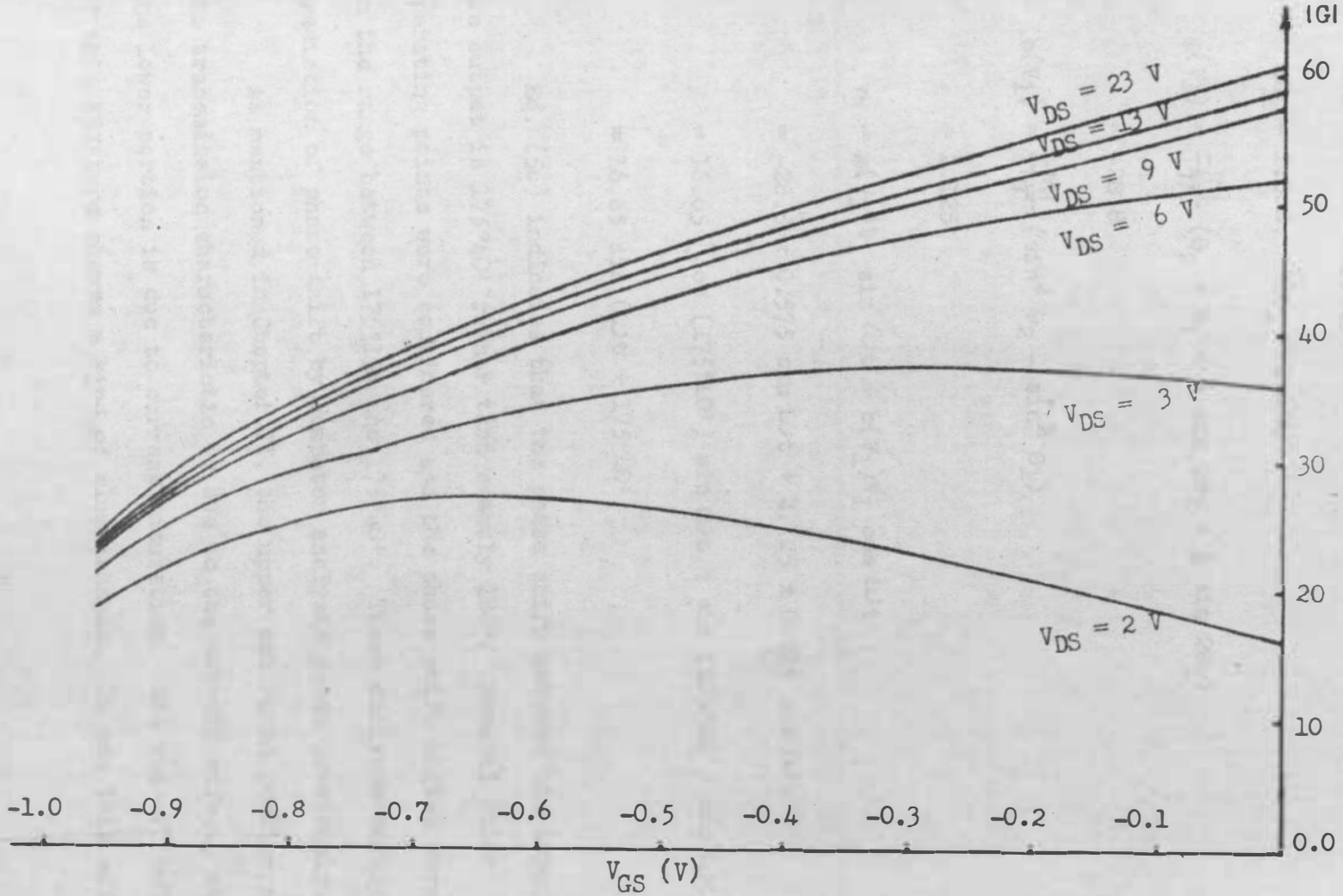

Figure 19. Magnitude of Amplification of the Designed Amplifier at f = 6250 Hz

$$\theta_2 = \sin^{-1} \frac{14 + 1.35}{19.45} = \sin^{-1} 0.790 = 0.904$$

$$2\theta_2 = 1.808, \quad 2\theta_1 = 1.414$$

$$g(V_1) = \frac{-|G|}{\pi} (\theta_2 + \theta_1 + \tfrac{1}{2} \sin 2\theta_2 + \tfrac{1}{2} \sin 2\theta_1)$$

$$= -28.8$$

$$b(V_1) = \frac{+|G|}{\pi} (\sin^2 \theta_2 - \sin^2 \theta_1)$$

$$= 2.125$$

$$v_3 = g(V_1)V_1 \sin \omega t + b(V_1)V_1 \cos \omega t$$

$$= -28.8 \times 0.575 \sin \omega t + 2.125 \times 0.575 \cos \omega t$$

$$= 16.65 \left[\cos (175°40') \sin \omega t + \sin (175°40') \cos \omega t\right]$$

$$= 16.65 \sin (\omega t + 175°40') \qquad (56)$$

Eq. (56) indicates that the phase shift between the input and the output is 175°40' rather than exactly 180°. Several other operating points were considered and the phase shift angles were all in the range between 175°15' and 175°40'. These analyses verify the prediction of phase shift by computer analysis given previously.

As mentioned in Chapter II, the upper saturated portion of the transmission characteristic is due to the cut-off effect, and the lower portion is due to current saturation. The cut-off behavior of this FET type showed a kind of sluggishness. It was this effect

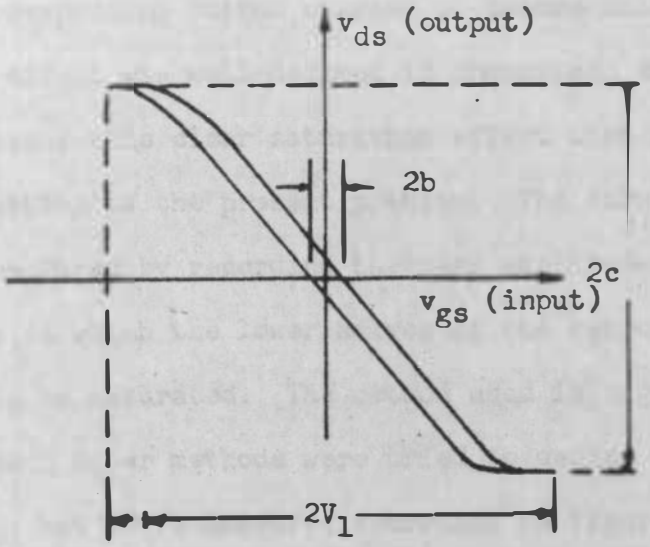

Figure 20. Transmission Characteristic Appeared on Type 503 Oscilloscope Screen at V_{GS} = - 0.8 V, V_{DS} = 16 V, G = 33.85, V_1 = 0.575 V, f = 6250 Hz, b = 0.04 V, c = 14 V

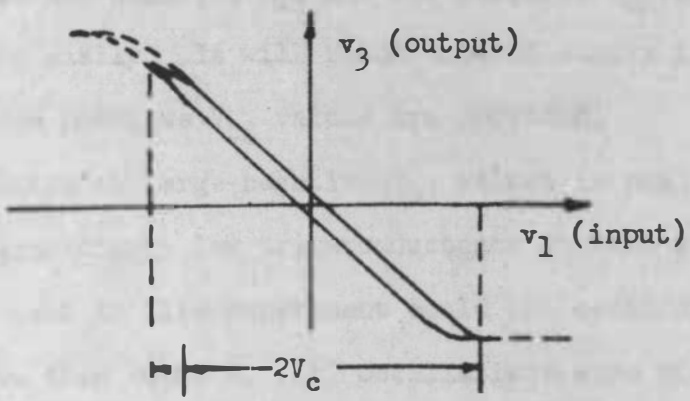

Figure 21. Method Used to Measure Critical Voltage

that caused some uncertainty in measuring the critical input voltage V_c at which the corresponding output started to become cut-off. The current saturation effect was well-defined in comparison with the cut-off effect. It was this clear saturation effect that provided the clue to the solution of the present problem. The curves shown in Figure 22 were measured by recording the peak amplitudes of the gate-source signals at which the lower halves of the output waves started to appear to be saturated. The method used is suggested in Figure 21. Several other methods were tried to define the critical voltage V_c, but those measured according to Figure 21 and shown in Figure 22 seemed to yield the best results.

Figure 22 reveals that increased negative gate-source bias V_{GS} and increased drain-source bias V_{DS} permit the larger critical voltages. This can be easily reasoned by referring to Figure 14. A signal operating at low negative V_{GS} and low positive V_{DS} values will reach saturation easily. It will reach cut-off easily if large negative V_{GS} and large positive V_{DS} values are provided.

The amplification at large negative V_{GS} values is small because of the correspondingly low transconductance in that region. The 2N3819 specimen used in this experiment could not oscillate at any V_{GS} more negative than -0.88 V. All oscillations were either partial saturation or full saturation. The method used to distinguish the partial saturation from full saturation was by judgment of the transmission characteristic appearing on the screen of an oscilloscope.

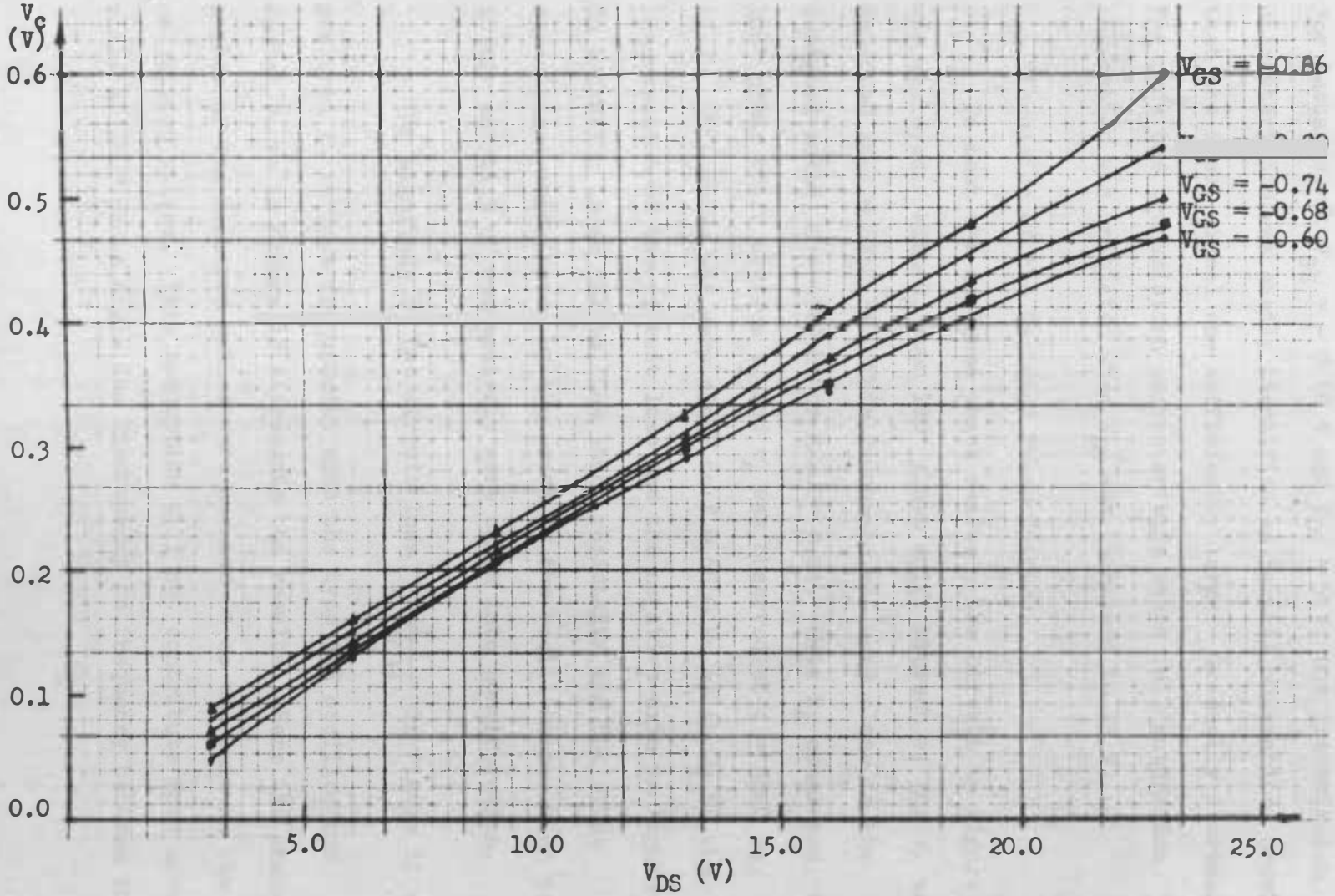

Figure 22. Critical Input Voltage Versus Operating Point of the Designed Amplifier

For instance, at $V_{GS} = -0.68$ V and $V_{DS} = 9$ V, the transmission characteristic was easily identified as partial saturation, provided that the input signal was sufficiently large. Gradually increasing V_{DS} made the transmission characteristic reach full saturation. Full saturation was initiated when V_{DS} was increased to 13 V.

C. Discussion of the Designed Phase Shifter

To test the designed phase shifter, the circuit in Figure 11 was employed. With R_g open 180° phase shift between v_3 and v_4 was observed at f = 6740 Hz. This frequency was very close to the designed value, f = 6720 Hz or $RC\omega = 2.45$. With R_g connected, the 180° phase shift between v_3 and v_4 was observed at f = 6880 Hz. Again, this value was very close to f = 6840 Hz as shown by the intersection of the circuit loss and the negative axis in Figure 12. In measuring these values, the shunt resistance and the shunt capacitance contributed by the probe of the oscilloscope which were 10 MΩ and 11.5 pf respectively were taken into consideration.

The magnitude of the circuit loss $\frac{1}{H_2(j\omega)}$ in Figure 11 was measured at various frequencies with the type 503 oscilloscope. The dashed curve in Figure 12 represents the results. Here the phase angles of the measured values were assumed to be the same as the calculated values. This assumption will not contribute much error since at 180° phase angle the discrepancy in frequency between the

calculated value and the measured value was only $\frac{6880 - 6840}{6840}$ or 0.6%.

If the phase shift between the input and the output was exactly 180° for the designed amplifier, the corresponding oscillation would occur at $RC\omega = 2.45$; i.e., $\left|\frac{1}{H_2(j\omega)}\right| = 29.0$ with R_g open, or $\left|\frac{1}{H_2(j\omega)}\right| = 30.2$ with R_g included. From the analysis of transmission characteristic, the phase shift between the input and the output was approximately 170°30' or $RC\omega = 2.28$ as given by Figure 12. The corresponding circuit loss of the phase shifter was 25.5.

With reference to Eq. (41), the describing function of the limiter at oscillation should be

$$H = \left|\frac{1}{G(j\omega)H_2(j\omega)}\right| = \frac{25.5}{|G(j\omega)|} \qquad (57)$$

D. Discussion of the Results

Eq. (53) indicates that the describing function of the limiter, H, can be approximated by the curves shown in Figure 13 depending upon the nature of the saturation. Therefore, from the value of H calculated from Eq. (57) with a known magnitude of amplification, the ratio $\frac{V_1}{V_c}$ can be found from these curves. Because of the low-pass filtering effect, the signal between the gate and the source during oscillation is nearly a pure sinusoid. The peak

value of this signal, V_1, can be predicted from this knowledge of $\frac{V_1}{V_c}$. The value of V_c can be found from Figure 22 at a particular operating point. The corresponding fundamental peak value of the output should be approximately equal $|G| V_1$. Here $|G|$ is the magnitude of amplification at the corresponding operating point.

The predicted peak amplitudes of v_{gs}, V_1, are shown in Figure 23. Here $\left|\frac{1}{H_2(j\omega)}\right|$ takes the value of 25.5 as shown in Figure 12 at $RC\omega = 2.28$ and $|G(j\omega)|$ can be found from Figure 19 at the corresponding operating point. The describing function (curve A in Figure 13) and critical voltages (Figure 22) are utilized.

Although the partial saturation transmission characteristic did occur, the predictions of V_1 with curve B in Figure 13 were larger than experimental values presented in Figure 24. For instance, for $H = 0.85$ the ratio $\frac{V_1}{V_c}$ calculated from curve A in Figure 13 is 1.34 but that given by curve B is 1.71. Predictions using curve A for the partial saturation cases gave results close to experimental values in Figure 24. For this reason all predictions in Figure 23 were based on curve A in Figure 13, regardless of the type of saturation, partial or full.

The variations of V_1 with operating point measured with the oscillation circuit of Figure 8 are shown in Figure 24. The

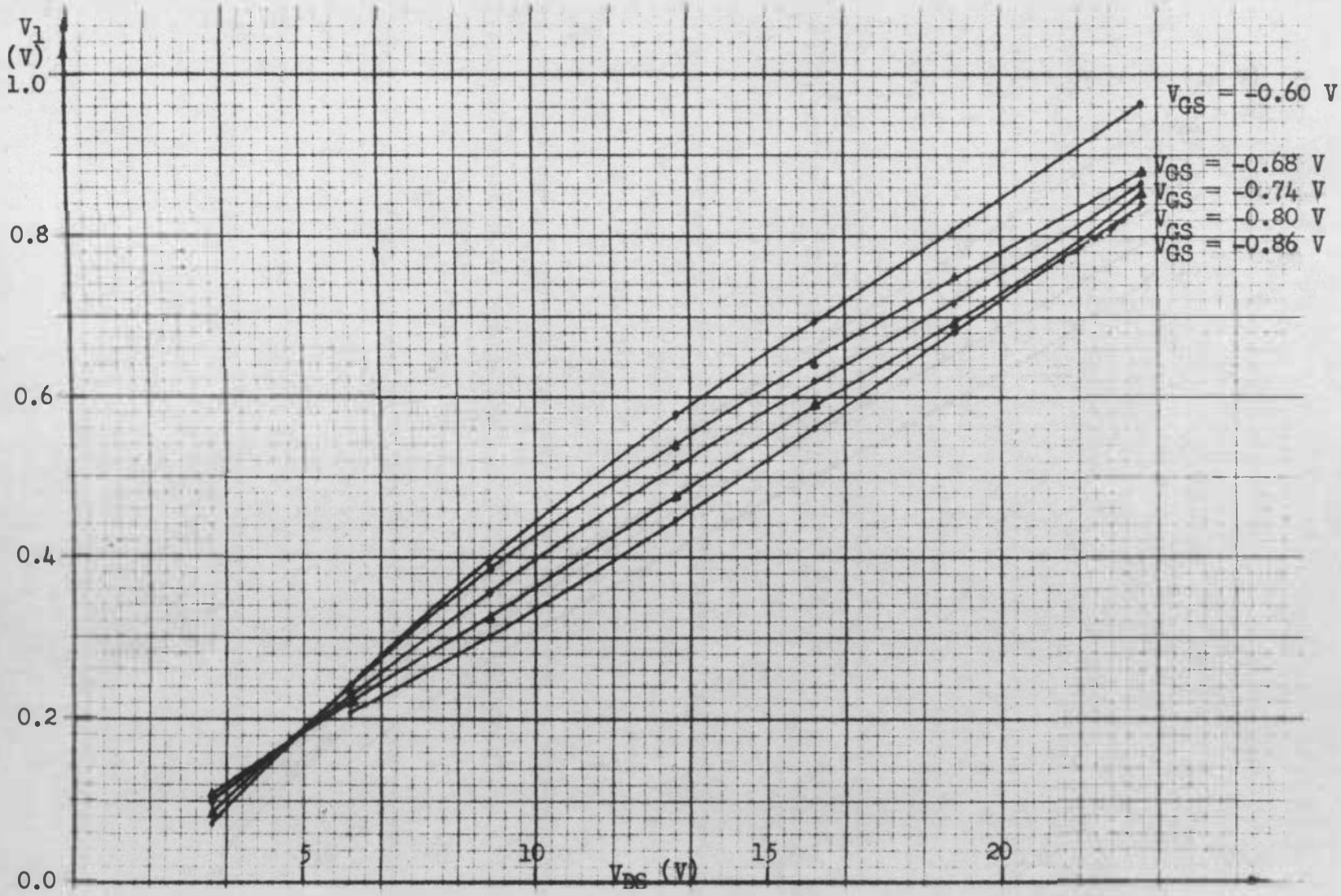

Figure 23. Predicted Peak Amplitudes of Gate-Source Signal of the Designed Oscillator

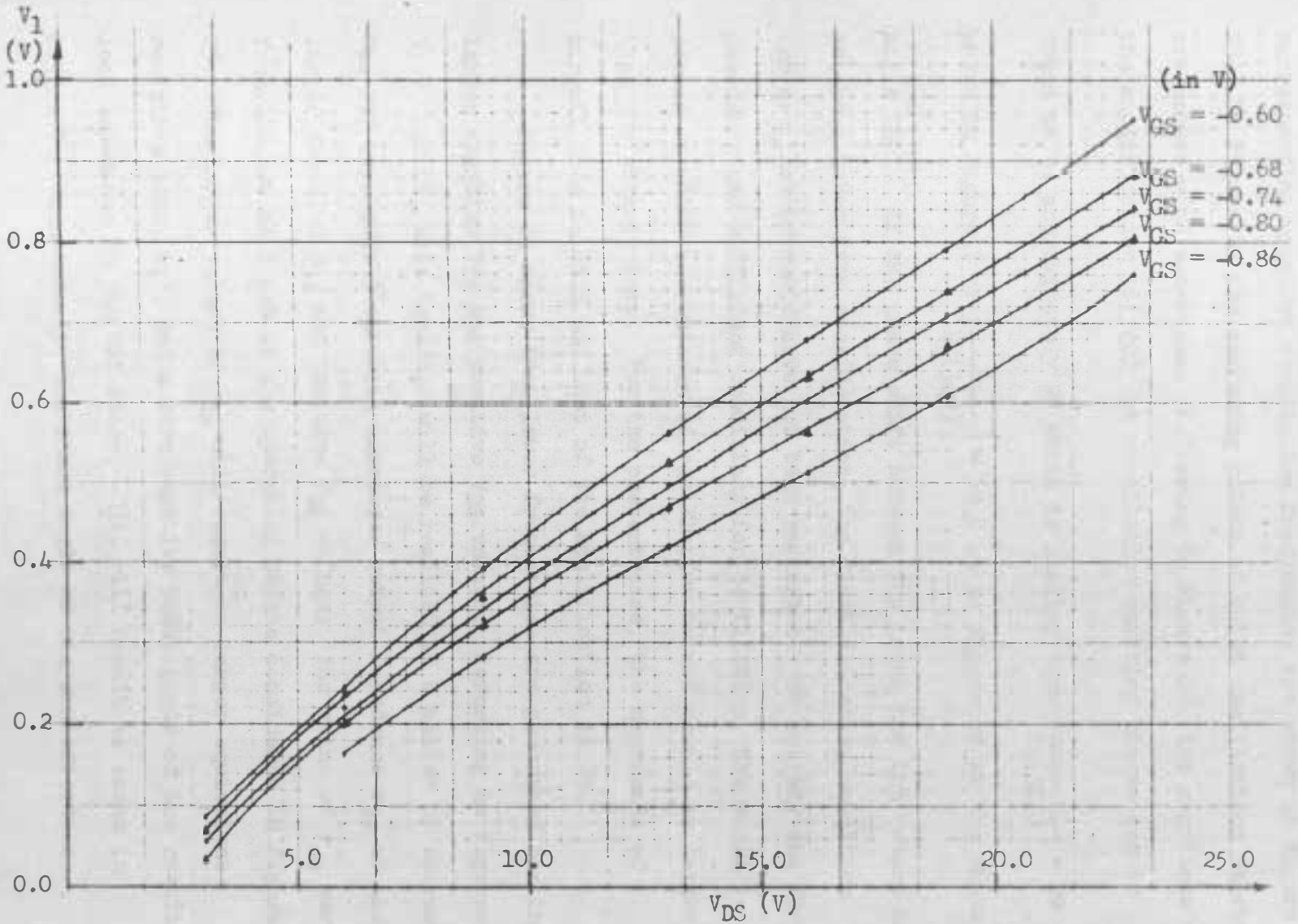

Figure 24. Experimental Values of Peak Amplitudes of Gate-Source Signal of the Designed Oscillator

corresponding measured oscillation frequencies are shown in Figure 25. In Figure 25 the operating points at which oscillations started are marked with asterisks. Referring to Figure 19, the magnitude of the amplification $G(j\omega)$ at oscillation starting biases can be found to be approximately 28 which is smaller than $\left|\frac{1}{H_2(j\omega)}\right| = 29$ shown in Figure 7 or $\left|\frac{1}{H_2(j\omega)}\right| = 30.2$ as in Figure 12 at the phase angle 180°. If the phase shift between the input and the output had not been taken into consideration, the first necessary condition for oscillation would have not been satisfied. To satisfy the first necessary and sufficient conditions for oscillation, the amplification at which the buildup of oscillation occurs should be larger than the circuit loss. For the present case, the magnitude of circuit loss is 25.5 and that of the amplification is 28.

Figure 25 shows that lower frequencies are generated for the larger negative V_{GS} and positive V_{DS} values. Referring to Figures 5, 9, and 18, this tendency will be realized as a matter of course. The FET type 2N3819 exhibits increased output impedance r_{ds} at the larger negative V_{GS} and positive V_{DS} values. The value of r_{ds} varies from 100 kΩ to 1 MΩ at the operating points considered in Figure 25. The larger values of r_{ds} will result in larger equivalent resistive load, R_2', and a more negative phase angle of the resultant load impedance on the FET stage, $-\psi$, will result as shown in Figure 9. Consequently, the phase angle of the amplification

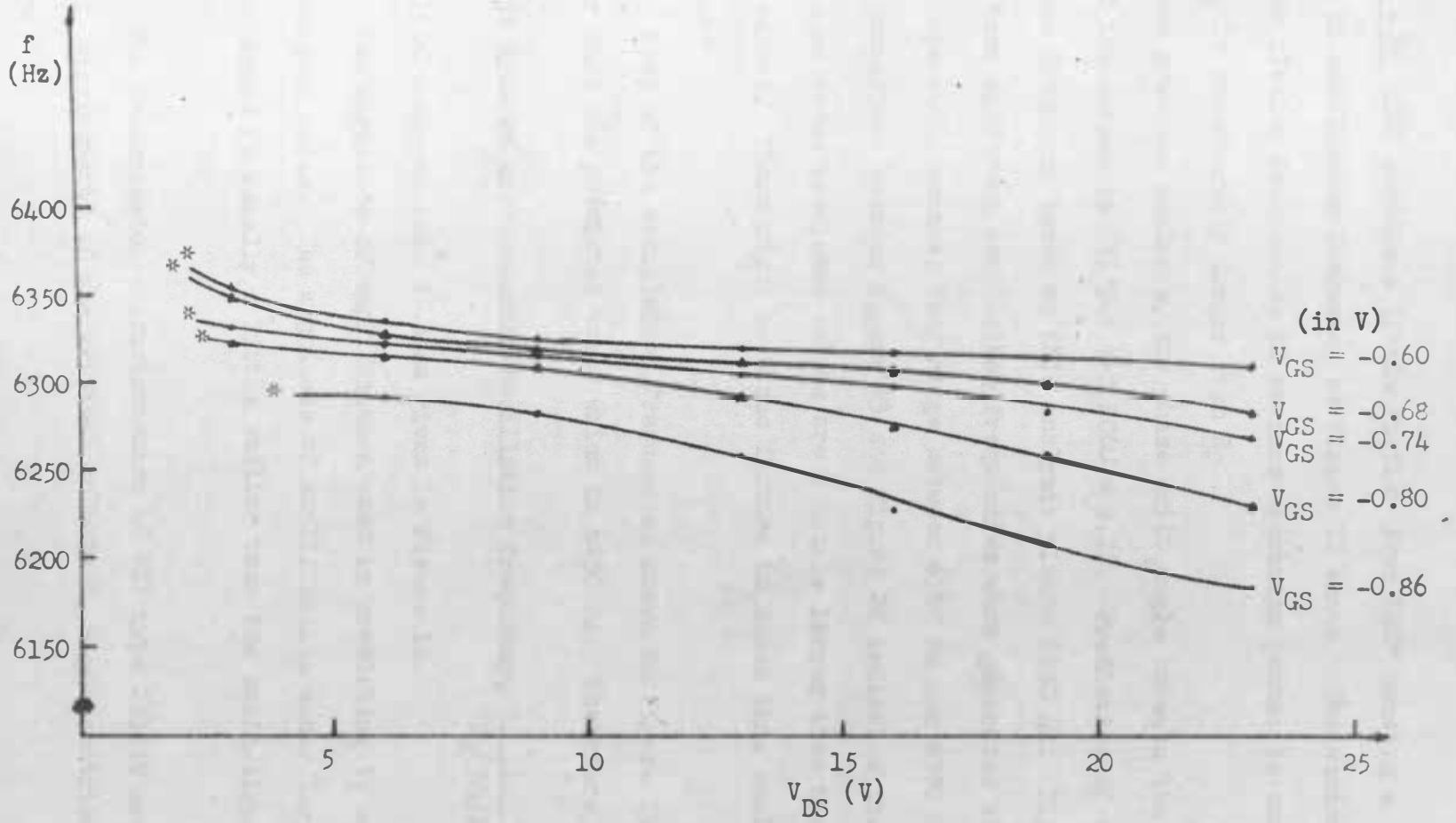

Figure 25. Experimental Variation of Oscillation Frequencies Versus Operating Points with Capacitor C = 1160 pf

$|G|\angle 180° - \psi$ will deviate a little further from 180° causing a decrease in oscillation frequency as Figure 12 shows. The variation of the oscillation frequencies at various operating points is small since r_{ds} is considerably larger than R_2 .

From previous analysis, the phase shift angle between the input and the output is 175°30' and $RC\omega = 2.28$. Prediction of the oscillation frequency based on this analysis yields 6250 Hz. Figure 25 shows that different oscillation frequencies were generated at different operating points; they range between 6180 Hz and 6370 Hz.

A comparison between Figure 23 and Figure 24 indicates that almost all of these predicted values are a little larger than the measured values. There might be three factors to cause this small discrepancy:

1. Most of the oscillation frequencies shown in Figure 25 are higher than the predicted value which is 6250 Hz. Therefore, the circuit loss at corresponding oscillation frequency, $\left|\frac{1}{H_2(j\omega)}\right|$, may be a little larger than 25.5 as given in Figure 12.

2. The magnitude of amplification used in predicting V_1 was the small-signal value. The magnitude of amplification under large signal conditions is usually a little smaller than the small-signal value.

3. The transmission characteristics of FET type 2N3819 are not ideal. Measurements of the critical voltage V_c might contribute some error.

From Items 1 and 2, the actual values of the describing function of the limiter when oscillating, should be a little larger than predicted, because of the division of a larger circuit loss $\left|\frac{1}{H_2(j\omega)}\right|$ by a smaller magnitude of amplification $\left|G(j\omega)\right|$. The larger H will result in a smaller $\frac{V_1}{V_c}$ ratio according to Figure 13. In addition to this, the measurements of V_c contribute some error. Summing up these three factors, the small discrepancy between Figure 23 and Figure 24 is reasonable.

According to the previous analyses and experimental data, the designed oscillator oscillates at $RC\omega = 2.28$ or $f = 6250$ Hz. If the original designed oscillation frequency, 6720 Hz, is desired, correction of the capacitive elements of this circuit is necessary. With $RC'\omega' = 2.28$, the new capacitive element C' is

$$C' = \frac{2.28}{50 \times 10^3 \times 2 \times \pi \times 6720} = 1085 \text{ pf}$$

Figure 26 shows the result. The amplitudes of oscillation are not affected by this process as discussed previously.

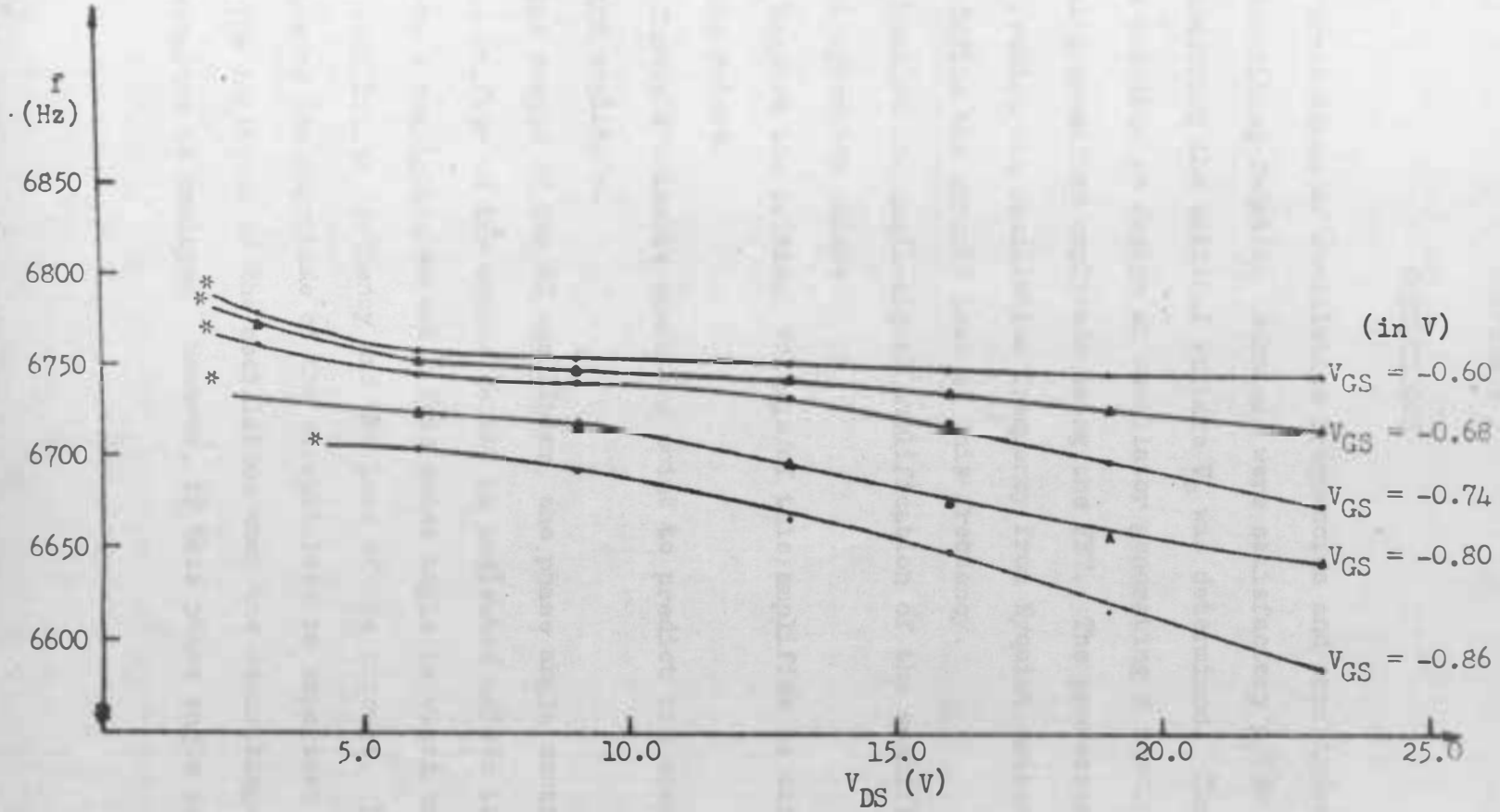

Figure 26. Oscillation Frequencies of the Designed Oscillator Versus Operating Points with Capacitor C = 1085 pf

CHAPTER V

CONCLUSIONS

The predictions of oscillation frequencies and amplitudes using the describing-function technique were satisfactory after a method of measuring the critical voltage V_c was determined. Therefore, it is possible to design an oscillator generating a specified frequency at a specified amplitude using the FET. The processes are:

1. Predict the oscillation frequency from Nyquist criterion.
2. Define the circuit loss at this frequency.
3. Measure the small-signal amplification of the amplifier at different operating points.
4. Measure the critical voltage of this amplifier at different operating points.
5. Choose a suitable operating point to predict the specified frequency and amplitude.

In the design of the RC oscillator, the phase angle contributed by the phase shifter to the system cannot be neglected unless it can be reduced to a negligible extent. This phase angle is vital in predicting oscillation frequency and the loss of the circuit. The correct value of the magnitude of the circuit loss is important in predicting the amplitude of the oscillation when the describing-function technique is employed. However, if this phase angle is

smaller than 10°, its effect on the hysteresis loop of the transmission characteristic generally can be neglected.

Figure 25 and Figure 26 show that the designed circuit oscillated in a range of frequencies at different operating points which produce different values of output impedance r_{ds} to change the effective phase shift angle of the amplifier. To reduce this effect, a different FET with higher transconductance g_m and higher output impedance r_{ds} may be used to replace the type 2N3819. If the new g_m is much higher than that of 2N3819, the load resistance R_2 in Figure 5 can be chosen to be much smaller than 20 kΩ and still can provide an amplification large enough to overcome the circuit loss. Under this situation, the effect of the variation of r_{ds} at different operating points will greatly reduce. Furthermore, if R_2 is also much smaller than Z_1 in Figure 5, the phase angle contributed by the RC phase shifter might be reduced to a negligible extent and the design work will be simplified.

REFERENCES

1. W. J. Cunningham, Nonlinear Analysis, McGraw Hill Book Co., Inc., New York, 1958, pp. 206-208, 301-305.

2. J. E. Gibson, Nonlinear Automatic Control, McGraw Hill Book Co., Inc., New York, 1963, pp. 197-198, 213-224, 229-231.

3. William Gosling, Field Effect Transistor Applications, 1965, pp. 1-8, 21-22, 27.

4. George Johnson, RF Harmonic Oscillator Discussion, Texas Instruments Incorporated, 1962.

5. F. C. Fitchen, Transistor Circuit Analysis and Design, D. Van Nostrand Co., Inc., 1966, pp. 18-21, 321-326.

6. H. J. Reich, Functional Circuits and Oscillators, D. Van Nostrand Co., Inc., 1961, pp. 371-373, 398.

7. S. S. Hakim, Feedback Circuit Analysis, John Wiley & Sons, Inc., 1965, pp. 210, 214.

8. L. J. Sevin, Jr., Field Effect Transistors, Texas Instruments Electronics Series, McGraw-Hill Book Co., Inc., New York, 1965, pp. 21-22, 51-53.

9. J. T. Wallmark and H. Johnson, Field-Effect Transistors, Physics, Technology and Applications, Prentice-Hall, Inc., 1966, pp. 1-4, 176-182.

10. J. D. Ryder, Electronic Fundamentals and Applications, Prentice-Hall, Inc., pp. 332-347.

11. Thomas R. Brown, Jr., Handbook of Operational Amplifier Active RC Networks, Burr-Brown Research Corporation, 1966, pp. 9-13.

APPENDIXES

APPENDIX A

A multivalued nonlinearity representing full saturation is shown in Figure 27-a. The corresponding fundamental components of the output $g(V_1)$ and $b(V_1)$ are given by

$$g(V_1) = \frac{1}{\pi V_1}\int_0^{2\pi} F(v_1)\sin\theta\, d\theta$$
$$b(V_1) = \frac{1}{\pi V_1}\int_0^{2\pi} F(v_1)\cos\theta\, d\theta \qquad (1)$$

The input is taken to be $v_1 = V_1 \sin\omega t$ and amplification to be G. The slope of the transmission characteristic is positive and equals $+|G|$

$$g(V_1) = \frac{2}{\pi V_1}\int_0^{\theta_2} |G|\,(V_1\sin\theta - b)\sin\theta\, d\theta + \frac{2}{V_1}\int_{\theta_2}^{\pi-\theta_1} C\sin\theta\, d\theta$$

$$+\frac{2}{\pi V_1}\int_{\pi-\theta_1}^{\pi} |G|(V_1\sin\theta + b)\sin\theta\, d\theta$$

$$= \frac{2}{\pi V_1}\int_0^{\theta_2} |G|\left[V_1\sin^2\theta - b\sin\theta\right] d\theta + \frac{2}{\pi V_1}\left[-C\cos\theta\right]_{\theta_2}^{\pi-\theta_1}$$

$$+\frac{2}{\pi V_1}\int_{\pi-\theta_1}^{\pi} |G|\left[V_1\sin^2\theta + b\sin\theta\right] d\theta$$

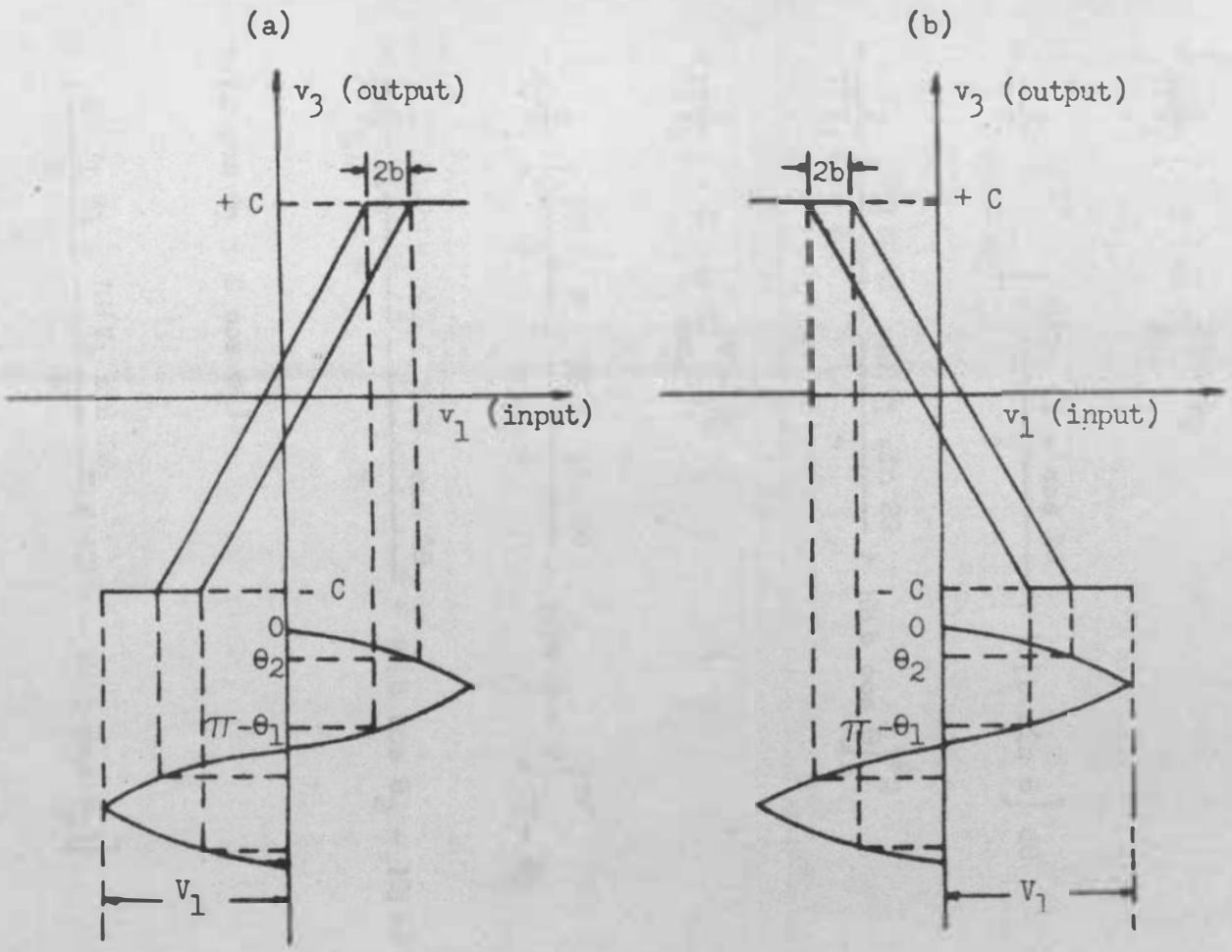

Figure 27. Full Saturation Transmission Characteristics with Phase Shift Effects

$$= \frac{2}{\pi V_1} \int_0^{\theta_2} \left[\frac{|G| V_1 (1 - \cos 2\theta)}{2} - |G| b \sin \theta \right] d\theta$$

$$+ \frac{2}{\pi V_1} \left[- C \cos \theta \right]_{\theta_2}^{\pi - \theta_1}$$

$$+ \frac{2}{\pi V_1} \int_{\pi - \theta_1}^{\pi} \left[\frac{|G| V_1 (1 - \cos 2\theta)}{2} + |G| b \sin \theta \right] d\theta$$

$$= \frac{2}{\pi V_1} \left[\frac{|G| V_1 \theta}{2} - \frac{|G| V_1 \sin 2\theta}{4} + |G| b \cos \theta \right]_0^{\theta_2}$$

$$+ \frac{2}{\pi V_1} \left[- C \cos \theta \right]_{\theta_2}^{\pi - \theta_1}$$

$$+ \frac{2}{\pi V_1} \left[\left(\frac{|G| V_1 \theta}{2} - \frac{|G| V_1 \sin 2\theta}{4} - |G| b \cos \theta \right]_{\pi - \theta_1}^{\pi}$$

$$= \frac{2}{\pi V_1} \left[\left(\frac{|G| V_1 \theta_2}{2} - \frac{|G| V_1 \sin 2\theta_2}{4} + |G| b \cos \theta_2 - |G| b \right) \right.$$

$$+ (C \cos \theta_1 + C \cos \theta_2)$$

$$\left. + \left(\frac{|G| V_1 \theta_1}{2} - \frac{|G| V_1 \sin 2\theta_1}{4} + |G| b - |G| b \cos \theta_1 \right) \right]$$

or

$$g(V_1) = \frac{|G| V_1}{\pi V_1}\left(\theta_2 + \theta_1 + \frac{\sin 2\theta_1}{2} + \frac{\sin 2\theta_2}{2}\right) + \frac{1}{\pi V_1}\left(-|G| V_1 \sin 2\theta_2\right.$$

$$\left. - |G| V_1 \sin 2\theta_1 + 2b|G| \cos \theta_2 - 2b|G| \cos \theta_1 + 2C \cos \theta_1\right.$$

$$\left. + 2C \cos \theta_2\right) \qquad (2)$$

But

$$2C \cos \theta_2 = 2|G|(V_1 \sin \theta_2 - b) \cos \theta_2 = 2V_1|G| \sin \theta_2 \cos \theta_2$$

$$- 2b|G| \cos \theta_2$$

$$= V_1|G| \sin 2\theta_2 - 2b|G| \cos \theta_2 \qquad (3)$$

$$2C \cos \theta_1 = 2|G|\left[V_1 \sin (\pi - \theta_1) + b\right] \cos \theta_1$$

$$= 2|G|\left[V_1 \sin \theta_1 + b\right] \cos \theta_1 = 2V_1|G| \sin \theta_1 \cos \theta_1$$

$$+ 2b|G| \cos \theta_1 = V_1|G| \sin 2\theta_1 + 2b|G| \cos \theta_1 \qquad (4)$$

Substitution of Eqs. (3) and (4) into (2) yields

$$g(V_1) = \frac{|G|}{\pi}\left(\theta_2 + \theta_1 + \frac{\sin 2\theta_2}{2} + \frac{\sin 2\theta_1}{2}\right) + \frac{1}{\pi V_1}\left[-|G| V_1 \sin 2\theta_2\right.$$

$$- V_1|G| \sin 2\theta_1 + 2b|G| \cos \theta_2 - 2b|G| \cos \theta_1 + V_1|G| \sin 2\theta_2$$

$$- 2b|G| \cos \theta_2 + V_1|G| \sin 2\theta_1 + 2b|G| \cos \theta_1$$

So,

$$g(V_1) = \frac{|G|}{\pi} \left(\theta_2 + \theta_1 + \frac{\sin 2\theta_2}{2} + \frac{\sin 2\theta_1}{2}\right) \tag{5}$$

where

$$\theta_1 = \sin^{-1} \frac{C - b|G|}{V_1|G|} \quad , \qquad \theta_2 = \sin^{-1} \frac{C + b|G|}{V_1|G|} \tag{6}$$

Similarly,

$$b(V_1) = \frac{2}{\pi V_1} \left[\int_0^{\theta_2} |G|(V_1 \sin \theta - b) \cos \theta \, d\theta + \int_{\theta_2}^{\pi - \theta_1} C \cos \theta \, d\theta\right.$$

$$\left. + \int_{\pi - \theta_1}^{\pi} |G|(V_1 \sin \theta + b) \cos \theta \, d\theta\right.$$

$$= \frac{2}{\pi V_1} \left[\left(\frac{|G| V_1 \sin^2 \theta}{2} - |G| b \sin \theta\right)\right]_0^{\theta_2} + \frac{2}{\pi V_1} \left[C \sin \theta\right]_{\theta_2}^{\pi - \theta_1}$$

$$+ \frac{2}{\pi V_1} \left[\left(\frac{V_1|G| \sin^2 \theta}{2} + b|G| \sin \theta\right)\right]_{\pi - \theta_1}^{\pi}$$

$$= \frac{2}{\pi V_1} \left[\frac{V_1|G| \sin^2 \theta_2}{2} - b|G| \sin \theta_2 + C \sin \theta_1 - C \sin \theta_2\right.$$

$$\left. - \frac{V_1|G| \sin 2\theta_1}{2} - b|G| \sin \theta_1\right]. \tag{7}$$

But $C = |G|\ (V_1 \sin \theta_2 - b)$ or $C = |G|\ (V_1 \sin \theta_1 + b)$ (8)

Substitution of Eq. (8) into (7) yields

$$b(V_1) = - \frac{|G|}{\pi} (\sin^2 \theta_2 - \sin^2 \theta_1) \tag{9}$$

For the case of the transmission characteristic shown in Figure 27-b the only modification needed in Figure 27-b is the substitution of $-|G|$ for $+|G|$ in Eqs. (5) and (9). The results are

$$g(V_1) = - \frac{|G|}{\pi} (\theta_2 + \theta_1 + \frac{\sin 2\theta_2}{2} + \frac{\sin 2\theta_1}{2}) \tag{10}$$

$$b(V_1) = \frac{|G|}{\pi} (\sin^2 \theta_2 - \sin^2 \theta_1) \tag{11}$$

Here $- C = - |G|\ (V_1 \sin \theta_2 - b)$ and

$$- C = - |G| \left[V_1 \sin (\pi - \theta_1) + b \right] \tag{12}$$

Rearrange Eq. (12), the results will be the same as those in Eq. (6), i.e.,

$$\theta_2 = \sin^{-1} \frac{C + b|G|}{V_1 |G|} \quad \text{and} \quad \theta_1 = \sin^{-1} \frac{C - b|G|}{V_1 |G|} \tag{13}$$

If there is no hysteresis loop, the quantity b can be set to zero and θ_1 will be the same as θ_2.

$$g(V_1) = - \frac{2|G|}{\pi} (\theta_1 + \sin \theta_1 \cos \theta_1) \tag{14-a}$$

$$b(V_1) = 0 \tag{14-b}$$

If there is no hysteresis loop and V_1 is also very much larger than V_c, then b, θ_2, and θ_1 can be all set to zero and the integration of $g(V_1)$ will result in $\frac{-4|G|V_c}{\pi}$ or

$$H = \frac{4V_a}{\pi} \tag{14-c}$$

APPENDIX B

Consider the case shown in Figure 28-a.

$$g(V_1) = \frac{1}{\pi V_1}\left[\int_0^{\frac{\pi}{2}} |G|(V_1 \sin\theta - b)\sin\theta\, d\theta\right]$$

$$+ \frac{1}{\pi V_1}\left[\int_{\frac{\pi}{2}}^{\pi - \theta_1} |G|(V_1 - b)\sin\theta\, d\theta\right]$$

$$+ \frac{1}{\pi V_1}\left[\int_{\pi - \theta_1}^{\pi + \theta_2} |G|(V_1 \sin\theta + b)\sin\theta\, d\theta\right]$$

$$+ \frac{1}{\pi V_1}\left[\int_{\pi + \theta_2}^{\pi - \theta_3} (-C \sin\theta)\, d\theta\right]$$

$$+ \frac{1}{\pi V_1}\left[\int_{2\pi - \theta_3}^{2\pi} |G|(V_1 \sin\theta - b)\sin\theta\, d\theta\right]$$

$$= \frac{|G|}{\pi V_1}\int_0^{\frac{\pi}{2}}\left[\frac{V_1(1 - \cos 2\theta)}{2} - b\sin\theta\right] d\theta$$

$$+ \frac{|G|}{\pi V_1}\left[(V_1 - b)(-\cos\theta)\right]_{\frac{\pi}{2}}^{\pi - \theta_1}$$

$$+ \frac{|G|}{\pi V_1}\int_{\pi - \theta_1}^{\pi + \theta_2}\left[\frac{V_1(1 - \cos 2\theta)}{2} + b\sin\theta\right.$$

$$+ \frac{C}{\pi V_1}\left[\cos\theta\right]_{\pi + \theta_2}^{2\pi - \theta_3}$$

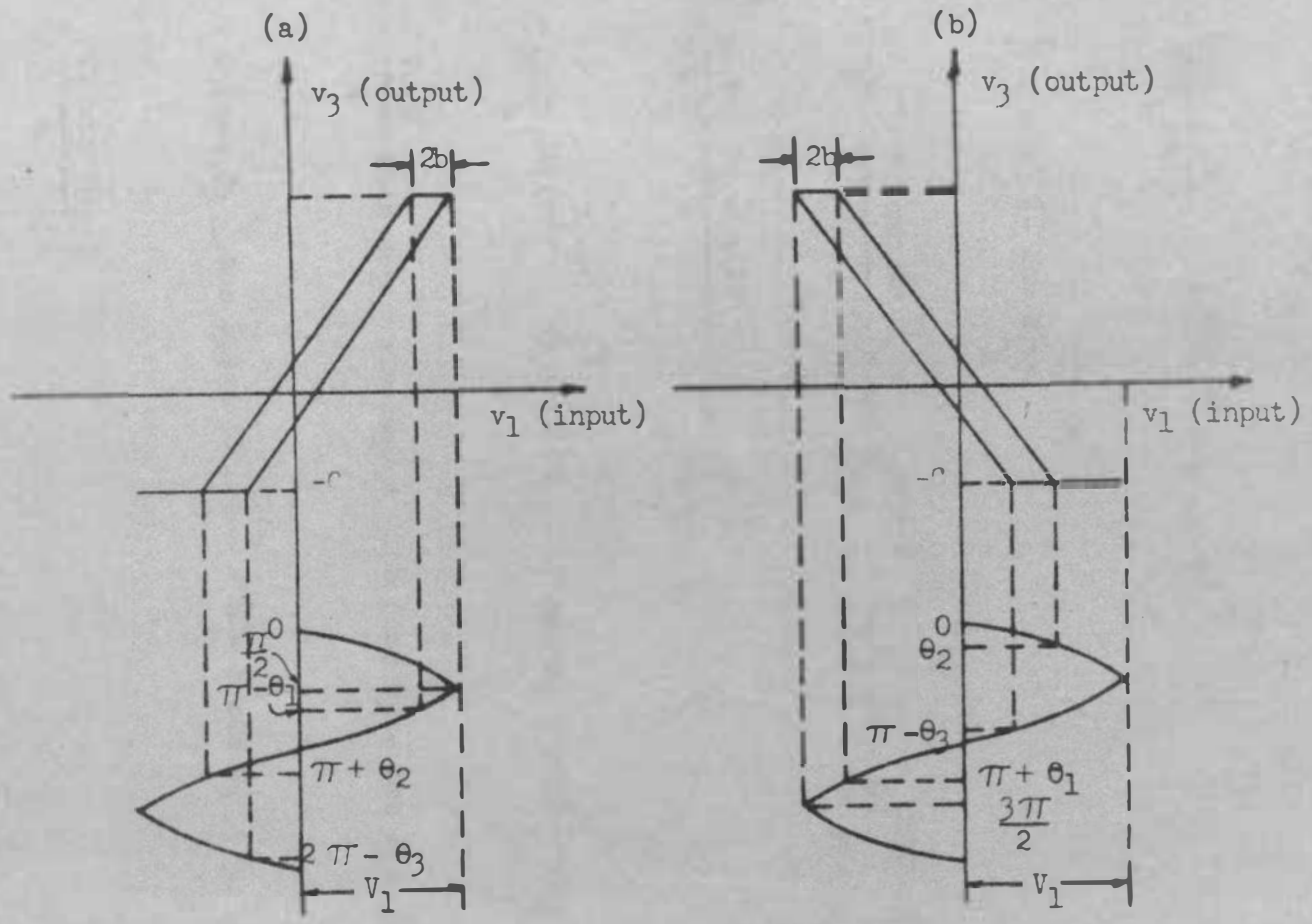

Figure 28. Partial Saturation Transmission Characteristics with Phase-Shift Effects

$$+\frac{|G|}{\pi V_1}\int_{2\pi-\theta_3}^{2\pi}\left[\frac{V_1\,(1-\cos 2\theta)}{2}-b\sin\theta\right]d\theta$$

$$=\frac{|G|}{\pi V_1}\left\{\left[\frac{V_1\theta}{2}-\frac{V_1\sin 2\theta}{4}+b\cos\theta\right]_{0}^{\frac{\pi}{2}}\right.$$

$$+\left[(V_1-b)(-\cos\theta)\right]_{\frac{\pi}{2}}^{\pi-\theta_1}$$

$$+\left[\frac{V_1\theta}{2}-\frac{V_1\sin 2\theta}{4}-b\cos\theta\right]_{\pi-\theta_1}^{\pi+\theta_2}+\frac{C}{|G|}\left[\cos\theta\right]_{\pi+\theta_2}^{2\pi-\theta_3}$$

$$\left.+\left[\frac{V_1\theta}{2}-\frac{V_1\sin 2\theta}{4}+b\cos\theta\right]_{2\pi-\theta_3}^{2\pi}\right\}$$

$$=\frac{1}{\pi V_1}\left\{|G|\left(\frac{V_1\pi}{4}-b\right)+|G|(V_1-b)\cos\theta_1+|G|\left[\frac{V_1}{2}(\theta_2+\theta_1)\right]\right.$$

$$-\frac{V_1|G|}{4}(\sin 2\theta_2+\sin 2\theta_1)+|G|b(\cos\theta_2-\cos\theta_1)$$

$$+C(\cos\theta_3-\cos\theta_2)+|G|\left[\frac{V_1\theta_3}{2}+b-b\cos\theta_3\right.$$

$$\left.\left.-\frac{V_1\sin 2\theta_3}{4}\right]\right\} \qquad (15)$$

where

$$2b=V_1-V_1\sin(\pi-\theta_1)\quad\text{or}\quad\sin\theta_1=\frac{V_1-2b}{V_1} \qquad (16)$$

Similarly,

$$V_1 \sin(\pi + \theta_2) = \frac{-C}{|G|} - b \quad \text{or} \quad \sin\theta_2 = \frac{C + |G|b}{V_1|G|} \tag{17}$$

and $$\sin\theta_3 = \frac{C - |G|b}{V_1|G|} \tag{18}$$

By eliminating $|G|b$ from Eqs. (17) and (18), it is easy to get

$$C = \frac{V_1|G|(\sin\theta_2 + \sin\theta_3)}{2} \tag{19}$$

From Eq. (16),

$$b = \frac{V_1(1 - \sin\theta_1)}{2} \tag{20}$$

Substitution of Eqs. (19) and (20) into Eq. (15), it results in a simplified form:

$$g(V_1) = \frac{|G|}{2}\left[\frac{\pi}{2} + (\theta_1 + \theta_2 + \theta_3) + \sin\theta_1\cos\theta_1 + (1 - \sin\theta_1)(\cos\theta_2 - \cos\theta_3) + \sin(\theta_2 + \theta_3)\right] \tag{21}$$

Substitution of Eqs. (19) and (20) into Eq. (17) yields

$$\sin\theta_1 + \sin\theta_2 - \sin\theta_3 = 1 \tag{22}$$

$$b(V_1) = \frac{1}{\pi V_1}\left[\int_0^{\frac{\pi}{2}} |G|(V_1\sin\theta - b)\cos\theta\, d\theta + \int_{\frac{\pi}{2}}^{\pi - \theta_1} |G|(V_1 - b)\cos\theta\, d\theta\right.$$

$$+ \int_{\pi - \theta_1}^{\pi + \theta_2} |G| (V_1 \sin\theta + b) \cos\theta \, d\theta$$

$$+ \int_{\pi + \theta_2}^{2\pi - \theta_3} (- C \cos\theta) \, d\theta$$

$$+ \int_{2\pi - \theta_3}^{2\pi} |G| (V_1 \sin\theta - b) \cos\theta \, d\theta \Big]$$

$$= \frac{1}{\pi V_1} \Big[\int_0^{\frac{\pi}{2}} \Big(\frac{|G| V_1 \sin 2\theta}{2} - |G| b \cos\theta \Big) d\theta$$

$$+ \int_{\frac{\pi}{2}}^{\pi - \theta_1} |G| (V_1 - b) \cos\theta \, d\theta$$

$$+ \int_{\pi - \theta_1}^{\pi + \theta_2} \Big(\frac{|G| V_1 \sin 2\theta}{2} + |G| b \cos\theta \Big) d\theta$$

$$- \int_{\pi + \theta_2}^{2\pi - \theta_3} C \cos\theta \, d\theta$$

$$+ \int_{2\pi - \theta_3}^{2\pi} \Big(\frac{|G| V_1 \sin 2\theta}{2} - |G| b \cos\theta \Big) d\theta \Big]$$

$$= \frac{1}{\pi V_1} \Big\{ \Big[\frac{- |G| V_1 \cos 2\theta}{4} - |G| b \sin\theta \Big]_0^{\frac{\pi}{2}}$$

$$+ |G| (V_1 - b) \Big[\sin\theta \Big]_{\frac{\pi}{2}}^{\pi - \theta_1}$$

$$+\left[\frac{-|G|V_1\cos 2\theta}{4}+|G|b\sin\theta\right]_{\pi-\theta_1}^{\pi+\theta_2}$$

$$-\left[C\sin\theta\right]_{\pi+\theta_2}^{2\pi-\theta_3}$$

$$+\left[\frac{-|G|V_1\cos 2\theta}{4}-|G|b\sin\theta\right]_{2\pi-\theta_3}^{2\pi}\Bigg\}$$

$$=\frac{1}{\pi V_1}\left[\frac{|G|V_1}{2}-b|G|+|G|(V_1-b)(\sin\theta_1-1)\right.$$

$$-\frac{|G|V_1\cos 2\theta_2}{4}+\frac{|G|V_1\cos 2\theta_1}{4}-|G|b\sin\theta_2$$

$$-|G|b\sin\theta_1+C\sin\theta_3-C\sin\theta_2-\frac{|G|E_1}{4}$$

$$\left.+\frac{|G|V_1\cos 2\theta_3}{4}-b|G|\sin\theta_3\right] \qquad (23)$$

Substitution of Eqs. (19) and (20) into Eq. (23) and simplification yields

$$b(V_1)=\frac{-|G|}{2\pi}\left[\frac{1}{2}+\frac{1}{2}(\cos 2\theta_1+\cos 2\theta_2-\cos 2\theta_3)\right.$$

$$\left.+(\sin\theta_2+\sin\theta_3)(1-\sin\theta_1+\sin\theta_2-\sin\theta_3)\right] \qquad (24)$$

Changing the analysis of the Figure 28-a into the partial saturation transmission characteristic with a phase shift a little smaller

than 180° (as in Figure 28-b) gives

$$g(V_1) = \frac{-|G|}{\pi}\left[\frac{\pi}{2} + (\theta_1 + \theta_2 + \theta_3) + \sin\theta_1 \cos\theta_1 \right.$$

$$\left. + (1 - \sin\theta_1)(\cos\theta_2 - \cos\theta_3) + \sin(\theta_2 + \theta_3)\right] \quad (25)$$

$$b(V_1) = \frac{|G|}{2\pi}\left[\tfrac{1}{2} + \tfrac{1}{2}(\cos 2\theta_1 + \cos 2\theta_2 - \cos 2\theta_3)\right.$$

$$\left. + (\sin\theta_2 + \sin\theta_3)(1 - \sin\theta_1 + \sin\theta_2 - \sin\theta_3)\right] \quad (26)$$

and

$$\theta_1 = \sin^{-1}\frac{V_1 - 2b}{V_1}, \quad \theta_2 = \sin^{-1}\frac{C + |G|b}{V_1|G|}, \text{ and}$$

$$\theta_3 = \sin^{-1}\frac{C - |G|b}{V_1|G|} \quad (27)$$

For the case the hysteresis loops in Figure 28 disappear; then $b = 0$, $\theta_1 = \frac{\pi}{2}$ and $\theta_2 = \theta_3$. Eqs. (25) and (26) become

$$g(V_1) = -|G|\left[\tfrac{1}{2} + \frac{1}{\pi}(\theta_2 + \sin\theta_2 \cos\theta_2)\right] \quad (28\text{-a})$$

$$b(V_1) = 0 \quad (28\text{-b})$$

For partial saturation case V_1 is small, because this occurs only when V_{DS} is not large enough to cause full saturation at oscillation. Therefore, it is not necessary to evaluate the value of $g(V_1)$ with V_1 much larger than V_c as was done in Eq. (14-c).